Quadruple abnormal protein aggregates in brainstem pathology and exogenous metal-rich magnetic nanoparticles. The substantia nigrae is a very early target in young urbanites and the gastrointestinal tract likely a key brainstem portal.

Lilian Calderón-Garcidueñas MA, MD, PhD [1, 2], Angélica González-Maciel MS[3], Rafael Reynoso-Robles BS[3], Jessica Hammond M.Sc.[4], Randy Kulesza PhD[5], Ingolf Lachmann PhD[6], Ricardo Torres-Jardón PhD[7], Partha S. Mukherjee PhD[8], Barbara A Maher PhD[4]

[1]The University of Montana, Missoula, MT 59812, USA

[2] Universidad del Valle de México, 14370, México

[3] Instituto Nacional de Pediatría, 04530, México

[4] Centre for Environmental Magnetism and Paleomagnetism, Lancaster Environment Centre, University of Lancaster, Lancaster, UK, LA1 4YQ

[5] Auditory Research Center, Lake Erie College of Osteopathic Medicine, Erie, PA, USA.

[6]AJ Roboscreen GmbH, Leipzig, Germany 04129

[7]Centro de Ciencias de la Atmósfera, Universidad Nacional Autónoma de México, UNAM, Mexico City, 04510 Mexico

[8] Indian Statistical Institute, Kolkata, 700108, India

Correspondence to: Professor Lilian Calderón-Garcidueñas, MA, MD, PhD, University of Montana, 32 Campus Drive, 287 Skaggs Building, Missoula, MT 59812, USA. Tel.: 406-243-4785; lilian.calderon-garciduenas@umontana.edu

Funding: This work was partially supported by E022 Instituto Nacional de Pediatría (AGM). B A Maher receives funding from Jaguar LandRover.

Abstract

Fine particulate air pollution ($PM_{2.5}$) exposures are linked with Alzheimer's and Parkinson's diseases. AD and PD neuropathological hallmarks are documented in children and young adults exposed lifelong to Metropolitan Mexico City air pollution; together with high frontal metal concentrations (especially iron)–rich nanoparticles (NP), matching air pollution combustion and friction-derived particles. Here, we identify aberrant hyperphosphorylated tau, α synuclein and TDP-43 in the brainstem of 186 Mexico City 27.29±11.8y old residents. Critically, substantia nigrae (SN) pathology seen in mitochondria, endoplasmic reticulum and neuromelanin (NM) is co-associated with the abundant presence of exogenous, Fe-, Al- and Ti-rich NPs.The SN exhibits early and progressive neurovascular unit damage and mitochondria and NM exogenous engineered Ti-rich nanorods, also identified in neuroenteric neurons. Such reactive, cytotoxic and magnetic NPs may act as catalysts for reactive oxygen species formation, altered cell signaling, and protein misfolding, aggregation and fibril formation. Hence, pervasive, airborne and environmental, metal-rich and magnetic nanoparticles may be a common denominator for quadruple misfolded protein neurodegenerative pathologies affecting urbanites from earliest childhood. The substantia nigrae is a very early target and the gastrointestinal tract (and the neuroenteric system) likely key brainstem portals. The ultimate neural damage and neuropathology (Alzheimer's, Parkinson's and TDP-43 pathology included) could depend on NP characteristics and the differential access and targets achieved via their portals of entry,thus where you live, what air pollutants you are exposed to, what you are inhaling and swallowing from the air you breath, what you eat, how you travel, and your occupational longlife history are key. Control of NP sources becomes critical.

Keywords: α-Syn, Alzheimer, brainstem, cerebellum, children, energy-dispersive X ray analysis EDX, nanoparticles, hyperphosphorylated tau pτ, iron, protein misfolding, Mexico City, neuromelanin, neuroenteric system, substantia nigrae, Alpha-synucleinopathies, $PM_{2.5,}$ portal of entry, tauopathies,titanium,Ti-rich nanorods, aluminum, TDP-43 proteinopathies, Parkinson.

1.Introduction

Exposure to air pollutants has increasingly been associated with the most common neurodegenerative diseases affecting millions of people across the world: Alzheimer's and Parkinson's. [1- 21] Neuropathological evidence shows that Alzheimer's disease (AD) is developing and progressing in children, teens and young adult residents of Metropolitan Mexico City (MMC). [15-16] In a forensic consecutive autopsy cohort of 203 MMC previously clinically healthy individuals (age 25.36 ± 9.23 y), all, except a 22y female with a TLR4 Asp299Gly polymorphism, exhibited AD hallmarks, as defined by the presence of phosphorylated tau protein (p-τ) and amyloid ß 17-24.[22- 29] Rapid progression to neurofibrillary tangle (NFT) stages III-V was documented in ~25% of 30 - 40 y olds.

We have previously reported an overlap between the neuropathological hallmarks of AD and PD in young (≤ 40y) MMC residents, such hallmarks notably appearing in childhood. [9, 12-19, 30-34] Specifically, in a study of 179 MMC residents ≤40y of age, we have identified p-τ and Lewy neurites (LN) in the olfactory bulbs (OBs) of toddlers. [16] By the second decade (n:57), 84% of the OBs exhibited p-τ (48/57), 68% exhibited LNs and vascular amyloid (39/57) and 36% (21/57) diffuse amyloid plaques. The overlap of AD and PD hallmarks has been also documented within auditory and vestibular nuclei, together

with a marked dysmorphology in the ventral cochlear nucleus and the superior olivary complex.[13, 31] The progressive involvement of the brainstem auditory evoked potentials (BAEPs) reflects the early brainstem participation in the neuroinflammatory and neurodegenerative processes. The compensatory plasticity, and increased auditory gain, are important in identifying strong non-invasive biomarkers of Alzheimer Continuum and early PD. [18, 34-36]

As we have documented previously, young MMC residents are exposed lifelong to high levels of fine airborne particulate matter ($PM_{2.5}$) and ozone, above the USEPA standards and WHO guidelines; they have high frontal concentrations of metal (especially iron)–rich nanoparticles (NPs) which match air pollution particles formed by combustion and friction processes, such NPs are also evident within both the heart and the neuroenteric system. [14, 18, 37-39] The presence within key organelles of brain and heart cells of metal-rich, redox-active, and strongly magnetic NPs raises important questions regarding their potential role in the development of AD and PD and extra-neural pathology in MMC residents.[12-14, 17-19,37, 39-41] Low air pollution, age and gender matched controls have not shown neurodegenerative or heart pathology.[17,33,38]

Across the world, a significant proportion of the population (including US residents) lives near highly-trafficked roads, where they are exposed to traffic-related air pollution (TRAP), a major contributor to urban air pollution. [42- 45] MMC experiences high levels of TRAP, in addition to pollution emitted both from industrial and natural (wind blown, volcanic, forest fires and trash and stubble-burning) sources. Air pollutants associated with health impacts encompass a diverse range of components, including fine and ultrafine particulate matter ($PM_{2.5}$ and $PM_{0.1}$, respectively), containing diesel soot, transition metals, nitrogen oxides and particle-bound phases, such as polycyclic aromatic hydrocarbons

(PAHs).[42, 44, 45] Of these components, ultrafine particles ($PM_{0.1}$, i.e. < 100 nm) are increasingly implicated in a wide range of adverse health impacts.[46-47] Compared with larger particles, ultrafine particles are far more numerous, highly reactive, and able to gain access to all major organs of the body.[48-51]

Of particular concern, transition metal-rich NPs, such as those formed abundantly as combustion- and friction-derived nanoparticles (CFDNPs), may act as catalysts for formation of reactive oxygen species (ROS) and for protein misfolding, aggregation and fibril formation.[7, 10, 12,14-18, 32,33, 41, 53-63]

Here, we investigate AD and PD neuropathological hallmarks in the brainstem in young MMC residents, and their associations with the presence, location and composition of exogenous, metal-rich NPs in the brainstem and cerebellum. Damage to the brainstem and cerebellum will extensively alter key networks modulating autonomic function, arousal, motor control and emotions.[64 - 67]

We have three primary aims: 1. to document, by immunohistochemistry, brainstem (including substantia nigra) pathology in a collection of 186 MMC autopsy samples from individuals 27.29±11.8y, and specifically, the presence of p-τ, alpha-synuclein and DNA-binding protein TDP-43; 2. to quantify, by magnetic remanence measurements, the concentrations of ferromagnetic, iron-rich NPs in the substantia nigrae, tectum/tegmentum /periaqueductal gray (PAG) and cerebellum, in a representative subcohort (n:15, age 34.33±15.6y, range 12-71y); and 3) to achieve, in a pilot sample, the first *in situ* identification of the composition as well as the location, size and shape of exogenous NPs in the substantia nigra of a 32y old subject, randomly selected from the cohort. For the latter aim, in order to achieve the required spatial resolution, i.e. to image and analyse NPs within the sub-cellular environment at near-atomic resolution, we used high resolution

scanning and transmission electron microscopy (HRSTEM) and energy-dispersive X ray analysis (EDX). Precise early identification of NP composition, as well as size, location and concentration, are critical, since it will establish which organelles are targeted, the NP potential toxicity and the resultant biological impact upon key AD, PD and TDP-43 targets and connecting brainstem networks.

Our working hypothesis is that exposure to reactive metal-bearing NPs, abundant and pervasive in the urban atmosphere and environment, comprises a biologically plausible common denominator for fatal PD, AD and TDP-43 proteinopathies, starting in pediatric ages.

2.Materials and Methods

2.1 Study area air quality

MMC residents are exposed frequently and lifelong to high levels of particulate air pollution, arising from traffic- and industry-related emissions, combined with unfavourable meteorology (pollution-trapping inversions).Even by conventional measures (i.e. mass concentrations of fine particulate matter, $PM_{2.5}/m^3$), MMC residents are often exposed to pollution levels above World Health Organization (WHO) guidelines and US Environmental Protection Agency (USEPA) standards. The USEPA annual $PM_{2.5}$ standard of 12 $\mu g/m^3$ and 24-hour mean standard of 35 $\mu g/m^3$ have been exceeded across the MMC area for the last 16 years (Figure 1).[68- 74] Typically, the highest $PM_{2.5}$ concentrations occur in the NE sector, associated with intense industrial and heavy duty diesel traffic, and decrease towards the SW residential area.[42, 45, 69, 70, 74] Exposures to ozone (O_3) concentrations are also above the USEPA standards (annual fourth-highest daily maximum 8-hour concentration, averaged over 3 years) all year long.[73] All other criteria pollutants for MMC, including nitrogen

dioxide, sulfur dioxide and lead, displayed elevated levels prior to 2000, but have been at or below the current EPA standards in the last 20 years.

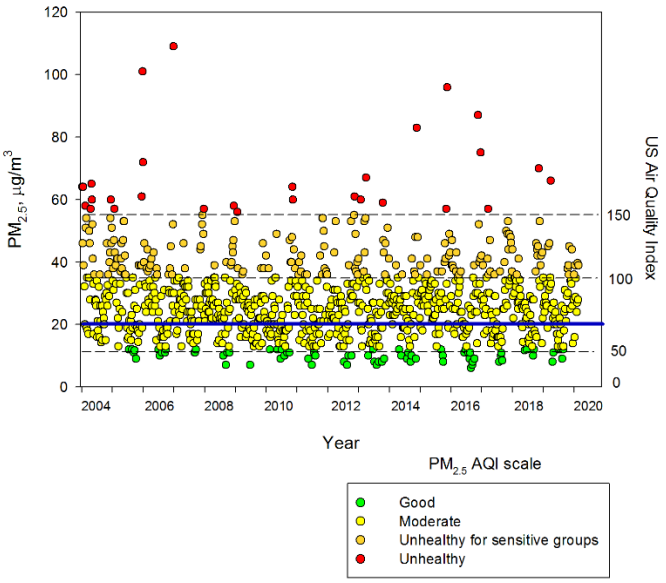

Figure 1. Trend of maxima PM $_{2.5}$ 24-hour average concentrations registered in all monitoring stations of the MMC from 2004 to April 2020 and their comparison against the WHO daily mean average (blue solid line) and the US Air Quality Index AQI. Data correspond to measurements from the manual PM network of the SEDEMA under a 6-day sampling schedule. Source: http://www.aire.cdmx.gob.mx/default.php#

In terms of health impact, however, it seems increasingly likely that ultrafine particles, of nanoscale dimensions (< 100 nm, so referred to here as nanoparticles, NPs), may pose a major risk. NPs are present in urban air in large numbers, are currently neither monitored nor regulated, and, notably, show little correlation with conventional mass concentration measurements, e.g. $PM_{2.5}$. At heavily trafficked roadsides, NP numbers can reach values in excess of 130,000/cm^3 (Dr. Maher personal communication, data measured in 2019, Manchester, U.K.). Although the majority (~90%) of airborne NPs consist of semi-volatile, carbon-bearing phases, the primary, solid, vehicle-derived NPs are often enriched in highly reactive transition metals, especially Fe, Cu, Mn, Ti and Cr and other metals including Ni, V, Pb and Zn.[75-77] Metal-bearing NPs are abundant in Mexico City air. More than 60%

of such NPs, collected and analyzed (n=572) by transmission electron microscopy, contain Fe, Pb or Zn.[78] Taking account of the abundance of NPs produced by vehicle brake wear [41], we describe such particles as combustion- *and* friction-derived nanoparticles (CFDNPs).

2.2 Study design and samples

One hundred and eighty-six forensic MMC autopsies, age 27.29±11.8y old (range 11 months to 40 years) were selected for this study, from sudden causes of death that did not involve the brain; all have previously been staged for AD and for olfactory bulb α synuclein, ß amyloid and pτ pathology.[15, 16] Autopsies were performed 3.7 ± 1.7 h after death. Cases were consecutive and included unrelated subjects with no pathological findings at the general autopsy other than the acute cause of death. Examination of autopsy materials was approved by the Forensic Institute in Mexico City and autopsies were performed in a five year period between 2004 and 2008. Brains were examined macroscopically, sections were selected for light and electron microscopy, and frozen tissues stored at minus 80°C until processed. Age, gender and Apolipoprotein E (APOE) status in Supplemental Table 1.

Brainstems were sectioned from the midbrain at the level of the superior colliculi to the lower medulla, with an average of 13.6±4.4 paraffin blocks and 48.7±12.0 slides per individual paraffin block examined. Paraffin embedded tissue was sectioned at a thickness of 7 μm and stained with hematoxylin and eosin (HE). Immunohistochemistry (IHC) was performed on serial sections as previously described.[15] Antibodies included: PHF-tau8 phosphorylated at Ser199-202-Thr205 (Innogenetics, Belgium, AT-8 1:1000), α-synuclein phosphorylated at Ser-129, LB509 (In Vitrogen, Carlsbad, CA 1:1000) and TDP43 mab2G10 (Roboscreen GmbH, Leipzig, Germany 1:1000). Examination for AD, alpha-

synucleinopathies and TDP-43 hallmarks in each brainstem included substantia nigrae. [22-24, 26-29, 79-87]

2.3 Transmission Electron Microscopy (TEM), High Resolution Scanning TEM (HRSTEM) and Energy Dispersive X Ray Analysis (EDX)

Separate sets of tissue blocks were prepared for initial, conventional bright-field TEM (osmium-stained) and for HRSTEM and EDX (no osmium staining); tissue sections were 100 nm thickness. The focus of the conventional TEM (JEOL-1011, Osaka, Japan, operated at 80 kV), of substantia nigrae, tectum, tegmentum, periaqueductal gray (PAG), and cerebellum, was observation of the integrity of the neurovascular unit and defining the location of the electrodense NPs present within target organelles and cell types and the sub-cellular pathology. In order to achieve detection and elemental analysis of intra-cellular NPs, high-angle annular dark field (HAADF) scanning transmission EM (STEM) was used (heavier elements displaying brighter contrast), in combination with multi-detection EDX. TEM grids (holey carbon films on nickel support grids) were randomly selected (2 from 10 grids), carbon-coated to prevent surface charging effects, and scanned using a FEI Titan3 Themis 300 STEM, operated at 300 kV. In identifying the elemental compositions of NPs by EDX (FEI Super-X 4-detector system), a probe current of 60 pA was used to acquire the elemental maps, in order to limit any beam-induced damage.

2.4 Magnetic remanence

For room-temperature measurements of saturation remanent magnetisation (SIRM), fresh/frozen tissue blocks were prepared by trimming of all external surfaces with a ceramic knife, to remove any possibility of external metallic contamination. All sub-sampling was done in a class II biological safety cabinet inside a class III biological laboratory. Surfaces and tools were treated with 70% ethanol. Inside the cabinet, air

throughflow was sampled using a Leland Legacy pump (SKC, Dorset UK) at 7.5 L/min through a magnetically-'clean' 1 μm PTFE filter, in order to quantify any airborne magnetic 'background' during the few minutes of in-cabinet tissue exposure during trimming/sampling. Once trimmed, each sample was subjected to freeze-drying (48 hours, Christ Alpha 2-4 LD plus) and placed in pre-measured sterilised polystyrene sample pots (10cc) for superconducting quantum interference device (SQUID) magnetometry (RAPID 2G DC magnetometer, 2G Enterprises, California USA; mean background noise level ~1 x 10^{-12} Am^2). All measurements were carried out at room temperature (293 K ±0.5 K) at the Centre for Environmental Magnetism and Palaeomagnetism, Lancaster University. First, the natural remanent magnetisation (NRM) of each sample was measured. Then, SIRMs were generated in a direct current (dc) magnetic field of 1 Tesla (T), using a Newport 4" Electromagnet Type A. All SIRM values were mass-normalized for freeze-dried brain weight (kg). The NRM or SIRM of all measurement materials (styrene pot, cling film) was measured for every individual sample, and subtracted, in order to isolate the SIRM of the tissue sample. Concentrations of magnetite in the brainstem samples were estimated from their SIRM values, using an experimentally-derived value of 11.5 Am^2 kg^{-1} for a pure magnetite powder, consisting of interacting, mixed, single domain and superparamagnetic (ave. diameter ~31 nm) magnetite particles.[88]

3. Results

3.1 Brainstem Neuropathology

The AD staging (pτ), substantia nigrae (SN) pτ and αSyn scoring, and the DNA-binding protein (TDP-43) results, are shown in Suppl Table 1. The earliest immunohistochemical findings in the brainstem of MMC children were pτ threads and neurites (NTs) in lower

medulla, followed by Lewy neurites (LNs), as described previously.[15, 16] Aβ data was taken from the two previous publications.[15, 16] When comparing the Alzheimer's staging from previous works and substantia nigrae pτ in the different age groups i.e., 0-20y, 21-40 and ≥41y olds, it is clear the presence of pτ in SN is an early and common finding. The presence of α synuclein in the SN was similar in the 0-20y and the 21-40y cohort (~20%) and increased in the older ≥40y cohort (n:7). On the other hand, TDP-43 abnormalities showed minimal variation within the 0-40y range. Immunocytochemical profiles of the 43-kDa transactive DNA-binding protein were characterized by loss of nuclear TDP-43 expression with powdery (dash-like) cytoplasmic particles[80, 85,86] associated with morphological changes of progressive degranulation of dopaminergic SNpc pars compacta neurons.

3.2 Representative substantia nigrae and brainstem Hyperphosphorylated tau (pτ), β amyloid, Alpha Synuclein, and DNA-binding protein TDP-43 Immunohistochemistry.

We documented α-Syn in 23% (n:42), 55% had pτ (n:100) and 18.68% (n:34) had TDP-43 (Suppl Table 1). Positive pτ neurites and nuclei in brainstem and SN were identified in toddlers (Figure 2A). TDP-43 pathology in a 11m old baby was identified in substantia nigrae pars compacta (SNpc) neurons and was characterized by isolated neurons with complete loss of nuclear TDP-43 expression (Figure 2 B, C). The same baby had diffuse Aβ plaques in frontal cortex (Figure 2D). Teens showed nuclear pτ in brainstem nuclei (i.e., oculomotor nucleus and accessory parasympathetic nucleus) and pτ neurites and nuclear positivity in SNpc (Figures 2E, F, G). Extensive arteriolar Aβ accumulation (amyloid angiopathy) was present in supratentorial cortical frontal and temporal lobes, along diffuse Aβ plaques (Figure 2 H, I). Alpha-synuclein positive neurites were previously seen in toddlers and young children in the lower brainstem, i.e., medulla [9, 12,16, 30, 31] while, here, SN

involvement and other nuclei (i.e., locus ceruleus, dorsal vagal nucleus), was extensively documented in teens (Figure 2J). TDP-43 pathology in the brainstem was characterized by dash-like immunopositive particles in the vicinity of the cell nucleus (Figure 2 K) with complete loss of nuclear TDP-43 expression.This type of pathology was mostly seen in lower brainstem levels,including medulla and pons and in relation to reticular formation intermediate and large cell neurons in the median column.Teens also showed the presence of glial cytoplasmic inclusions with a coiled-body like morphology (Insert in Figure 2K). Subjects in the third and fourth decades of life showed advanced lesions, i.e., 32 y old male (subject #20 in Table 1) with diffuse and mature Aβ plaques in frontal cortex (Figure 2L) with reactive GFAP astrocytes surrounding the plaques.Extensive pτ neurites and neurofibrillary tangles are seen in the SNpc of the same 36y old male as above.Alpha-synuclein positive granules were seen in SNpc in this 26y old female (#15 in Table 1) (Figure 2N and insert).While cytoplasmic α-Syn was a frequent finding, Lewy bodies were rare and associated with extensively degranulated neurons (Figure 2O).By the third decade, SNpc TDP-43 nuclear clearing with progressive neuron degranulation was in place (Figure 2P). TDP-43 pathology was observed in substantia nigrae, non-motor neurons including reticular nuclei, and pontine neurons with nuclear clearing and dash-like particles, but no neuronal somatic skein-inclusions. Pictures of abnormal SNpc neurons using hematoxylin and eosin H&E are seen in Figure 2 Q-Z to illustrate a common finding from childhood: neurons with typical hyaline cytoplasmic inclusions in 14y olds (T) surrounded by macrophages and extraneuronal deposits of NM, as the MMC resident gets older, the changes are striking(Figure 2Y,Z).

3.3 Substantia nigrae Electron Microscopy

TEM findings for the SN were remarkable in relation to early neurovascular unit pathology. Extensive breakdown of the neuropil was present around blood vessels with clusters of lipids, lipofuscin and vacuolated neuropil around vessel walls (Figures 3A, B). Perivascular neuropil breakdown and damaged axons were constant findings (Figures 3B, C). Rounded electrodense NPs were common in red blood cells (RBC) in close contact with endothelial cytoplasm in small vessels and inside endothelial cell nuclei (Figure 3D). The measurable size of the NPs in the SN was in the range of 9-60 nm (average 19± 6 nm).

SN neurons show progressive accumulation of neuromelanin (NM) starting at age 11 months (Figures 4A, B) and by age 12y, NM granules are already accumulating in paranuclear neuronal location (Figures 4C,D).Clusters of NPs were commonly associated with heterochromatin (Figures 4E,F). Strikingly, NPs were present in NM granules, dilated ER, abnormal mitochondria and in mitochondria in close contact with NM (Figure 4G, H(insert), I). Oligodendroglia showed adjacent large axons with myelin breakdown and contracted axons (Figure 4J). Fibrillary ill-defined structures were seen in the midst of NM with numerous NPs and twisted tubules (Figure 4K). Dilated ER, abnormal mitochondria and mitochondrial-endoplasmic reticulum (ER) contact sites (MERCs) were common in SN neurons (Figure 4L). In subjects in the 4th decade and beyond, the abundance of NM was striking (Figures 5A, B, C). Membranous, vesicular and lipid Lewy body-like structures were identified inside SN neurons. [87] (Figure 5D). SN blood vessels showed endothelial cells with abnormal tight junctions (TJs) (Figure 5E, F). Vascular β-pleated sheets were observed in blood vessels in close contact with lipofuscin (Figure 5H).Perineuronal macrophage-type cells were common around neurons (Figure 5 I), with numerous lysosomes, a rare one containing contain a lattice image with several layers of well ordered fringes with a perpendicular alignment (Figure 5J). Figure 6 illustrates the SN in the 32y

old male included in figures 7 and 8. Extensive damage to the SN NVU is seen with loss of perivascular astrocytic processes, and myelinated and unmyelinated axons. Macrophage processes surround one small blood vessel in the midst of neuropil breakdown (Figure 6A). NM is closely associated with NPs; mitochondria exhibited NPs both inside the matrix and in the double membranes (Figure 6B, C).

In order to identify the elemental composition of the observed intra-cellular, electrodense NPs, SN sections from a 32y male were additionally subjected to HRSTEM and EDX. HAADF-STEM images revealed the abundant presence of NPs, often in groups or clusters, in close association with mitochondrial structures and neuromelanin (Figures 7-9).

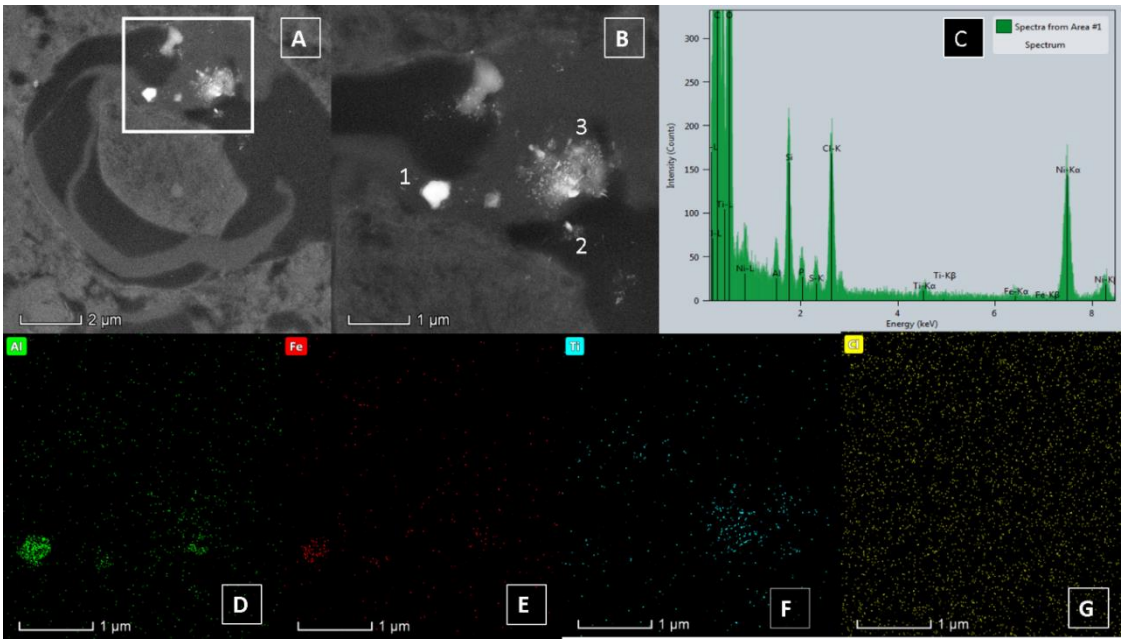

Figure 7 A, B. High magnification high-angle annular dark field-scanning/transmission electron microscopy (HAADF-STEM) of SN tissue, 32 y old subject (also please see Figure 8); B: a higher magnification image of the bright, electrodense NPs (marked as 1, 2 and 3) shown in the area in the white box in A. C. EDXA spectrum for the area shown in B. D – F. elemental maps for the area shown in B.

Figure 7 shows the presence of NP clusters, of different sizes, shapes and compositions, in close association with NM in the SN of this 32y old. Some NPs appear as rounded aggregates (NPs marked 1 and 2 in Figure 7B), dominantly composed of aluminium

(Figure 7D) and iron (Figure 7E). The cluster of smaller, distinctively elongate NPs (group 3 in Figure 7) is dominated by titanium (Figure 7F). The EDX spectrum, Figure 8C, displays additional marked peaks in silica and nickel, arising from the nickel TEM grid, and chlorine, which occurs all over the analysed area (Figure 7G), likely reflecting some aspect of sample preparation. Similar metal compositions are evident for NPs seen in association with, and apparently traversing, the double membrane of an SN mitochondrion (Figure 8). In addition to the rounded aggregates of aluminium- and iron-rich particles, discrete and elongate particles of titaniferous composition are evident (Figure 8 E, J).

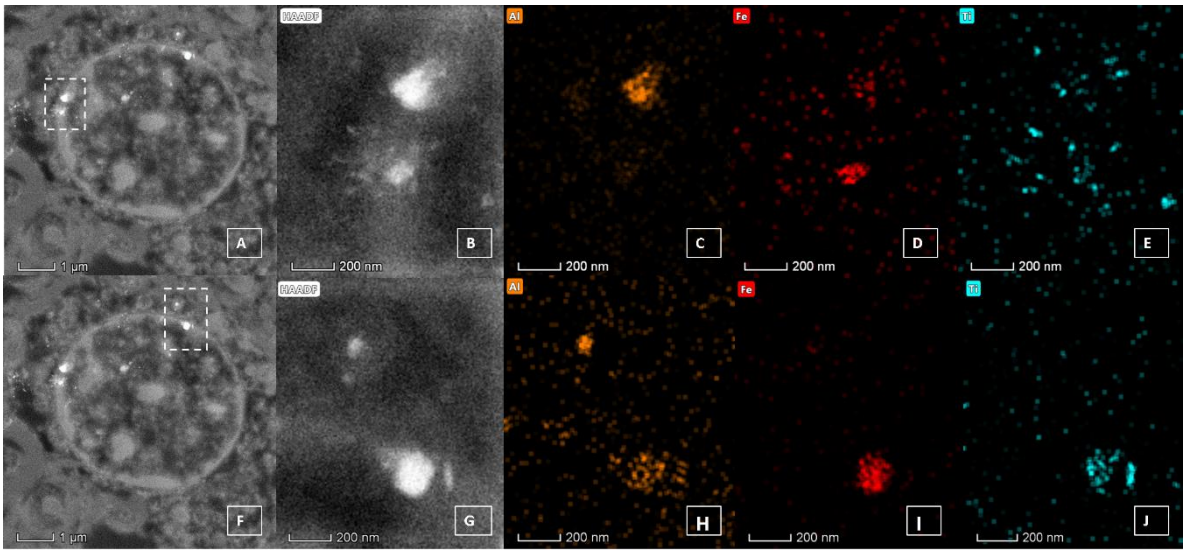

Figure 8. A and F: HAADF-STEM of NPs around a mitochondrion in SN tissue, 32 y old subject (B and G higher magnification images of the bright, electrodense NPs shown in the white box in A and F, respectively); C – E: elemental maps for the particles in the white box shown in A; H – J: elemental maps for the area shown in F.

These latter titanium-rich, acicular NPs are particularly distinctive; in our prior work on frontal tissue samples, we have not seen particles with this elongate morphology, nor have we observed them in urban roadside particulate air pollution samples. Conversely, we have observed similarly elongate, Ti-rich particles in neuroenteric tissue samples (Figure 9),

which, we infer, have been ingested and/or swallowed from airborne sources, and which have traversed the small bowel epithelium to access the neuroenteric pathway.

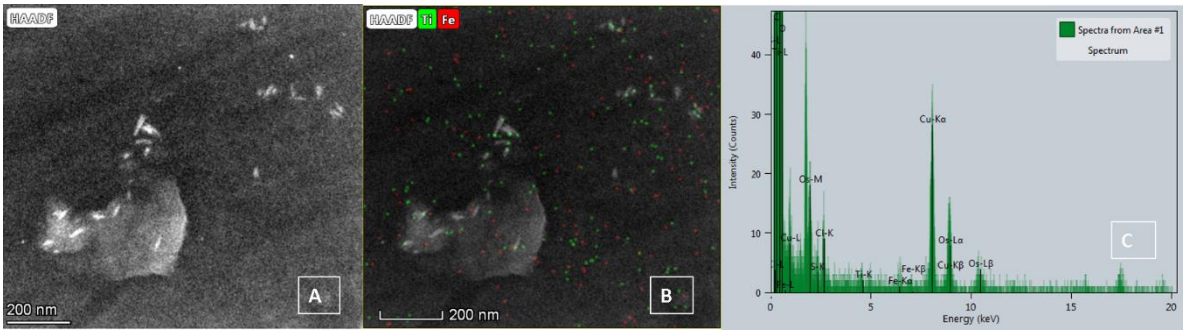

Figure 9A and B: HAADF-STEM of Ti-bearing elongated laths, in neuroenteric tissue sample from a 39y old male with both AD and PD hallmarks; C EDX spectrum for the area imaged in A and B (NB Cu peaks reflect the use of a copper TEM support grid).

3.4 Magnetic remanence

Figure 10 and Table 1 summarise the SIRM values for each of the SN, tectum, tegmentum, PAG and cerebellum tissue samples measured, versus age. Individual subjects display variable SIRMs, with little apparent correlation with age. However, the three brain regions (Figure 10A – C) display significant differences (Fig. 10 D, p-value = 0.0116) in their magnetic content. Median SIRM values (all $\times 10^{-6}Am^2kg^{-6}$) vary from 1.445 for SN samples, 2.97 for tectum/tegmentum/PAG, and 4.75 for cerebellum. The estimated ferrimagnetic concentration and numbers of magnetite-like NPs range from 0.02– 3.15 (median 0.11) µg/g dry wt and 0.22 to 39 (median 1.36) $\times 10^9$ /g, respectively for the measured SN samples; from 0.04 – 2.15 (median 0.22) µg/g dry wt and 0.53 to 26.65 (median 2.67) $\times 10^9$/g for the tectum/tegmentum/PAG samples; and from 0.03 – 2.63 (median 0.34) µg/g dry wt and 0.32 to 32.54 (median 4.26) $\times 10^9$/g for the cerebellum samples.

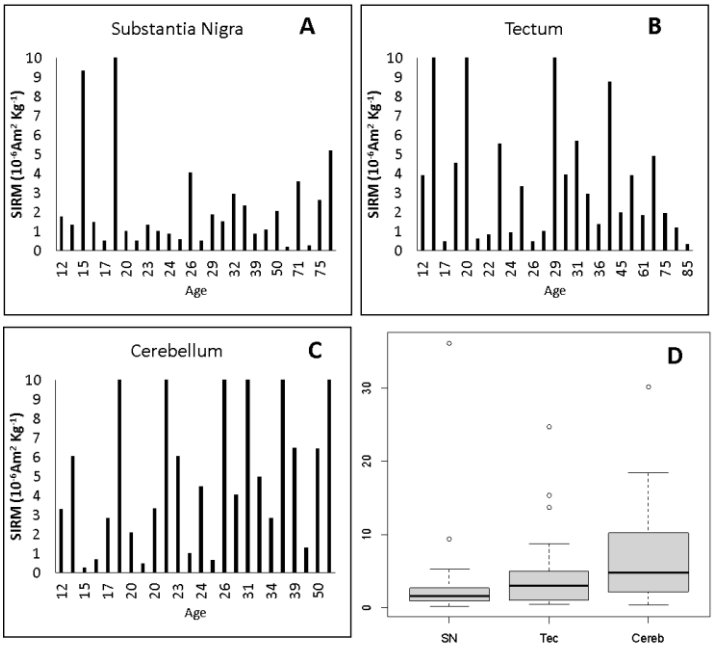

Figure 10. Room-temperature SIRM values versus age for A. SN samples, B. tectum/tegmentum/PAG, C. cerebellum, and D. box plots, showing significant differences between the magnetic content of the 3 regions (Kruska-Wallis test, p-value =0.0116).

ID#	Age	SIRM (10^{-6} Am^2 Kg^{-1})			Magnetite concentration µg/g			No. magnetite particles 10^9/g		
		SN	*TTP*	*CB*	*SN*	*TTP*	*CB*	*SN*	*TTP*	*CB*
1	12	1.8	3.92	3.31	0.13	0.28	0.24	1.61	3.52	2.97
2	15	1.36	13.7	6.05	0.10	0.99	0.44	1.22	12.30	5.43
3	15	9.37		0.3	0.68		0.02	8.41		0.27
4	17	1.52	0.5		0.11	0.04		1.36	0.45	
5	17	0.53	4.57		0.04	0.33		0.48	4.11	
6	20	36.23	15.32	10.16	2.63	1.11	0.74	32.52	13.75	9.12
7	20	1.02	0.63	2.11	0.07	0.05	0.15	0.91	0.57	1.89
8	20			0.5			0.04			0.45
9	20			3.37			0.24			3.02
10	22	0.52	0.87	30.2	0.04	0.06	2.19	0.47	0.78	27.11
11	23	1.37		6.07	0.10		0.44	1.23		5.45
12	24	1.02	5.55	1.03	0.07	0.40	0.08	0.92	4.99	0.93
13	24	0.89	0.95	4.49	0.07	0.07	0.33	0.80	0.85	4.03
14	26	0.6	3.37	0.69	0.04	0.24	0.05	0.54	3.02	0.62
15	26	4.08	0.49	11.72	0.30	0.04	0.85	3.67	0.44	10.52
16	27	0.53	1.02		0.04	0.07		0.47	0.92	
17	29	1.9	24.73		0.14	1.79		1.70	22.20	
18	31		3.97	4.08		0.29	0.30		3.56	3.66

19	31	1.54	5.72	15.93	0.11	0.41	1.15	1.38	5.13	14.30
20	32	2.95	2.97	5.01	0.21	0.22	0.36	2.65	2.67	4.50
21	34			2.84			0.21			2.55
22	35			14.25			1.03			12.79
23	36	2.35	1.39		0.17	0.10		2.11	1.25	
24	39	0.9	8.78	6.51	0.07	0.64	0.47	0.81	7.88	5.85
25	45	1.1	1.99	1.32	0.08	0.14	0.10	0.99	1.79	1.19
26	50	2.07	3.91	6.47	0.15	0.28	0.47	1.86	3.51	5.81
27	61	0.2	1.86		0.02	0.14		0.18	1.67	
28	71	3.62	4.92	18.46	0.26	0.36	1.34	3.25	4.42	16.57
29	75	0.29	1.96		0.02	0.14		0.26	1.76	
30	75	2.64	1.22		0.19	0.09		2.37	1.09	
31	85	5.23	0.34		0.38	0.03		4.69	0.31	

Table 1. Room temperature SIRM values for a representative sub-cohort of the MMC subjects, and calculated concentrations and number concentrations of magnetite NPs: SN = substantia nigra; TTP = tectum/tegmentum/PAG; CB = cerebellum.

4. Discussion

We are documenting in a collection of 186 brainstems from Mexico City residents age 27.29±11.8y old, the striking overlap of hyperphosphorylated tau, α synuclein and TDP-43- markers of AD and PD-, and, surprisingly, transactive response DNA-binding protein TDP-43 (a marker for amyotrophic lateral sclerosis (ALS) and frontotemporal lobar degeneration with ubiquitin-positive inclusions (FTLD-TDP)[89-96] strongly supporting a common denominator impacting the brain early in life. The brainstem and cerebellum are critical not only because they host key networks modulating autonomic function, arousal, motor control and emotions,[64-67, 97] but because damage to specific nuclei and network connections shed light on associated early clinical manifestations and critical portals of entry of our culprit: metal-rich exogenous nanoparticles.[98] The dominant presence of Fe, Al and Ti in the NPs present in substantia nigrae (SN) mitochondria, points unequivocally to their exogenous sources -including engineered Ti-rich nanorods-, and raising serious

concerns. TiO_2 NPs are widely manufactured for use in both domestic (e.g. cosmetics, sunscreens) and industrial (e.g. paints, coatings, electroceramics, solar cells) applications [99-101] and are abundant in E-waste.[51] Al-rich NPs are also abundant in airborne pollution, and, together with Fe and Ti, have been reported in high concentrations in Beijing residents' serum and pleural effusions.[102]

The SN presence of distinctive, acicular NPs of titanium-rich composition indicates that NPs have different portals of entry and subsequent transport routes - and, hence, potentially different brain targets. We have not previously observed elongate Ti-rich NPs in frontal or heart samples, nor in roadside airborne PM. Conversely, we have imaged and analysed similar particles in the neuroenteric system (myenteric plexus neurons), suggesting that these engineered NPs have accessed the brainstem via axonal transport, having traversed the gut wall after ingestion (e.g. with food) and/or being inhaled and swallowed. These observations are consistent with the key work of Holmqvist et al.,[103] showing the transport of αSyn via the vagal nerve to the dorsal motor nucleus of the vagus in a time-dependent manner, and the monosynaptic nigro-vagal connections discussed by Anselmi et al.[104, 105]

Notwithstanding the possibility of intra-cellular dissolution and (slow) clearance of exogenous particles[40] the brainstem metal-rich NPs may reflect the prevalence of those species in the environment to which these young urbanites have been exposed.[106] Specific metal cytotoxicity is evident from abundant *in vitro* and animal studies, e.g., TiO_2 NPs produce upregulation of miR-29b-3p reinforcing apoptosis, imbalance in the Th1/Th2 cells, small intestine physical(ileum) barrier structural changes in a dose-dependent manner, and epigenetic changes. [107-112, 55] Food sources of TiO_2 NPs are substantial[107], concentrations in food reportedly range from 3 to 2400 mg kg^{-1} with particle sizes between 30 to 410 nm.

Peters et al.[110] described in 15 human autopsies abundant TiO_2 particles in ileum > jejunum> kidney>spleen>liver in the size range of 50-500 nm, modal size 100-160 nm and ~ 17% <100 nm.

It is remarkable, the distinctive, elongate Ti-rich nanorods observed in the SN and neuroenteric samples here differ from the mostly spherical TiO_2 common in food additives, and may instead reflect handling of, for example, e-waste, or plastics.[99, 100, 113]

In terms of Fe-rich, ferrimagnetic NPs, the amount of midbrain magnetite measured here varies from subject to subject, an expected finding for individuals with different NPs exposure levels. However, our observation that the amount of magnetite varies significantly between the three different brain regions examined here (cerebellum > tectum/tegmentum/PAG > SN) is striking. Gilder et al.'s [114] study of 7 formaldehyde-fixed brains displayed ~60 × lower magnetic contents, with little variation between the 7 subjects, but highest magnetite concentrations in olfactory bulb, brainstem and cerebellum. Our findings suggest that different NPs appear to have different portals of entry: Fe- and Al-rich NPs via inhalation and circulation and Ti-rich nanorods via neuroenteric axonal transport. Thus, it is possible that the significant differences in magnetite content seen here between the SN, tectum/tegmentum/PAG and cerebellum might reflect not only the nature of the anatomical structures (i.e.,cluster of SN neurons versus intraxonal flow in afferent and efferent fibers) but also differential targeting of specific brain regions and cellular targets by NPs with differing exogenous sources,chemical composition, size,shape and entry portals. Thence, the ultimate neural damage and neuropathological hallmarks incurred would depend both on the NP characteristics and the differential access and targets achieved via their portals of entry.

With regard to the SN, much published evidence demonstrates that both Fe-oxide and Ti-oxide NPs produce cytotoxicity and oxidative stress in specific targets including dopaminergic cells, leading to αSyn aggregation and fibrillation.[60, 115- 123]

No matter what the entry portal, the chronic delivery of exogenous Fe-rich NPs to the brain is likely to induce oxidative stress and neuroinflammation.[60, 55, 124, 125] Release of free Fe ions, e.g. within acidic lysosomal environments, can catalyse increased and uncontrolled production of reactive oxygen species (ROS) through the Fenton reaction [60, 55] and neuroinflammation.[125-129] The presence of strongly magnetic NPs in the brainstem and cerebellum, in number concentrations of up to 39×10^9/g (dry wt) tissue may carry additional and specific significance; not only providing a source of reactive Fe, but also acting synergistically to promote the toxicity of amyloid-β, as shown by *in vitro* studies.[130] Indeed, magnetite NPs have been found directly associated with senile plaques and amyloid-β fibrils in an AD brain[131], and may contribute directly to Alzheimer-like neurodegeneration changes.[132-134] Depending on their location, concentration, size, degree of aggregation and magnetic interactions between NPs, magnetite NPs might also damage target organelles and cells through hyperthermia and/or magnetic rotation effects. Because magnetite is an excellent absorber of microwave radiation at frequencies of between 0.5 and 10 GHz (cell phones, for example, operate at frequencies of ~1 – 2 GHz), localised heating effects might be induced. [135-138] That some organisms are able to detect and respond to cues from the Earth's magnetic field, through the presence of biologically formed magnetite NPs, is unequivocal.[139] We suggest that, depending on exposure, the variable ingress of exogenous, pollution-derived magnetite NPs to major organs, including the brain, may account for some findings[140-143] that extremely weak alternating magnetic fields (i.e. with magnetic field amplitudes in the μT and nT ranges), can induce statistically

significant effects in biological systems. If DNA synthesis, RNA transcription and cell signalling, Ca^{++} flux, for example, can be thus affected, then the magnetic responses of ~ 10^9 magnetite pollution NPs/g tissue may provide a further direct pathway to neurodegeneration.

In the SN, we observe associations between clusters of Fe- (and other metals)-rich NPs and endosomal structures like NM. Magnetic interactions between magnetite NPs can enhance their response to external magnetic fields, even for particles otherwise too small (< ~ 30 nm) to align at ambient temperature with applied magnetic fields.[88] Even at low concentrations, Fe-rich and TiO_2-NPs accelerate αSyn fibrillization, a matter of deep concern for individuals exposed to high concentrations of these airborne NP species,i.e., α-synuclein fibrils can grow at much lower monomer concentrations than that required for *de novo* fibril formation.[129, 144, 122] The NPs size is critical: in human neuroblastoma cells, 10 and 30 nm ferric oxide nanoparticles significantly depleted cellular dopamine, increased ROS, damaged the BBB and produced neuronal α-synuclein expression.[60]

Al-rich NPs in the SN is an interesting finding, Al has, of course, been one of the must studied environmental agents linked with AD, with observational studies indicating that aluminium levels are significantly elevated in brain, serum, and CSF of AD patients.[145] Our novel results are consistent, specifically, with Perl and colleagues' work who identified intraneuronal aluminum accumulations (10 – 50 × adjacent NFT-free neurons and controls) in hippocampal neurons bearing NFTs in AD patients.[146] Using a rabbit model, Perl & Good [147] showed that exposure to intranasal aluminum leads to direct uptake into the brain and distribution along olfactory pathways. *In vitro*, cytotoxic and genotoxic damage by Al_2O_3 NPs has been associated with Al^{3+} ion release in the acidic environment of vesicles.[148] Al-induced neurocognitive decline among Al occupational workers is a serious

hazard and downregulating PI3K, Akt, and mTOR1 expression and inducing neuronal cell death has been shown experimentally and in Al workers.[149] Exley and Clarkson[150] suggested that the Al content of brain tissue in Alzheimer's disease, autism spectrum disorder and multiple sclerosis is significantly elevated versus controls in a study of 191 tissue samples.

Several SN findings in this work are remarkable, including the mitochondrial and ER abnormalities, and the vesicular structures and dysmorphic organelles; the latter - as described by Shahmoradian et al., [87]surrounded by NM fragments. The observed accumulation of metal-rich NPs in association with the NM raises the issue reported by Haining and Achat-Mendes[151] of NM apparently conferring '*susceptibility to chemical toxicity by providing a large sink of iron-bound, heme-like structures in a pi-conjugated system'.* Zecca et al., and Zucca et al.'s excellent[152-153] papers describing the accumulation of neuromelanins in concentrations as high as 1.5-2.6 microg/mg tissue in putamen, cortex, cerebellum and a recent paper describing substantia nigrae membrane and matrix proteins characteristic of lysosomes at a lower number than in typical lysosomes, gave the authors an indication of a reduced enzymatic activity and impaired capacity for lysosomal and autophagosomal fusion. Highly relevant to our findings, Zucca and co-authors [153] suggested that: i. NM-containing organelles likely have impaired capacity for lysosomal and autophagosomal fusion; and ii. the accumulation of proteins of aggregation and degradation pathways supporting the ubiquitin-proteasome system is inadequate. Both suggestions are in accord with a dysfunctional autophagy and ubiquitin proteasome system (UPS) in turn implicated in protein aggregation and toxicity by Limanaqi et al.[154] Thus, in the case of young MMC residents, it is highly probable that the variable but extensive accumulation by

NM of highly oxidative (and magnetic), metal-rich NPs will accelerate the dopaminergic cell damage at earlier ages, and as documented here, children exhibit extensive damage to SNpc with macrophages phagocytizing neuromelanin loaded neurons. Activated microglia-mediated engulfment of dopaminergic neurons with abundant NM could increase neuroinflammation on one hand and alter their role in αSyn clearance and degradation on the other.[155] NPs engulfed by macrophages affect their phagocytosis and migration capabilities [156] and since macrophages are themselves a rich source of inflammatory mediators and matrix metalloproteinases, they can worsen tissue injury by producing ROS, inducing apoptosis, and exacerbating ischemic injury. [157]Our Figure 4H insert illustrates a SNpc common phenomenon: the intimate contact between endolysosomes (EL) and mitochondria, an issue Wang et al.,[158] discusses in the context of functional mitochondrial outer membrane permeabilization (MOMP) execution during cellular apoptosis signaling. Their exciting paper shows mitochondria are targeted by endolysosomes during MOMP and key to our electron microscopic observation: *interactions of ELs with mitochondria control BAX recruitment and pore formation (*most certainly an effective pathway to kill SNpc neurons).

Another mechanism to take into account relates to damage to nuclear membranes by NPs: dysregulation of the nucleocytoplasmic transport machinery regulated by the structure and function of nuclear pores and mRNA export mechanisms, could result in protein accumulation.[159] Leibiger et al., [160] have proposed that TDP-43 interferes with lysosomal function and its own degradation via lysosomal pathways triggering lethal autophagy. Indeed, common pathways are shared by a number of neurodegenerative diseases,

including dysregulation of RNA metabolism and pathological persistence of stress granules. [161,162]

Our observed magnetic concentrations, in the order SN<tectum/tegmentum/PAG< cerebellum, likely signal the circuits and systems affected by NP ingress, encompassing the SN and its connectivity-based parcellation with limbic, cognitive and motor arrangements. determining in part decisional and motor impulsivity, as described by Zhang et al.[65] PAG plays a key role in emotions-related cognitive processes and in neurovegetative regulation [66] while the cerebellum has a pivotal functional role in human affective processing.[67, 163, 164, 122, 165] The elevated concentrations of magnetite in the cerebellum are notable and recall the selective targeting of mercury intoxication. [166]

4.1 Significance of overlap of four distinct neurodegenerative markers in young pollution-exposed subjects.

The overlap of four distinct simultaneous neurodegenerative markers (pτ, Aβ,αSyn and TDP-43) present in 10.98% (20/182) of young MMC urbanites appears crucial; co-existence of markers of two relatively common diseases, sporadic AD and PD, with a less common amyotrophic lateral sclerosis (ALS) disease/ frontotemporal degeneration (FTD) suggests a common aetiological denominator. We strongly support mapping out the development of these fatal diseases in forensic autopsies of young people - without either clinical evidence and/or morbidities associated with neurodegeneration – enables characterization of the earlier neurodegenerative pathomechanisms taking decades to become openly clinical. Because NP pollution loadings and compositions will differ between different locations, even within the same city, similar investigations of young fatalities will permit definition in each city and each country of the populations at risk and

the identification of potential environmental and/or other factors in common.

Hyperphosphorylated tau was by far the most common misfolded protein in our subjects. Our TDP-43 immunohistochemistry findings in SN neurons and nonmotor brainstem nuclei are particularly worrisome (34/182 cases, 18.68%), given the young age of affected subjects: 26.8±10.5y. We have documented in the SN an overlap between TDP-43 pathology and αSyn in 20 cases and with p-τ in 30 subjects.Karanth and co-workers[167] in a study of 375 autopsies of demented Alzheimer disease pathology (tau and Aβ) subjects, age 86.9±8.0 with α-synuclein, and TDP-43 data, along with Braak neurofibrillary tangle stages I to VI, found 19.2% with quadruple misfolded proteins.Quadruple misfolded proteins patients had MMSE scores in the severe impairment range and higher odds of APOE4 status. The authors concluded: *Quadruple misfolded proteins appear to be a common substrate for cognitive impairment and to be associated with an aggressive course of disease that typically ends with severe dementia.*[167] They added a statement that is very important for our quadruple misfolding proteins findings in MMC children and young adults:The *prevalence of comorbid α-synuclein and TDP-43 with Alzheimer disease pathology (tau and Aβ) may complicate efforts to identify therapies to treat and prevent Alzheimer disease.*[167]We fully agreed with them.

Gesner et al.,[168] work posed a key question: Development of Neurodegeneration in Amyotrophic Lateral Sclerosis: From Up or Down? It is evident in our young subjects that the lower brainstem is an early TDP-43 pathology target as it involves the reticular formation in medulla, pons, midbrain and the SN. Moreover, we also documented glial cells with cytoplasmic positivity. Interestingly, Tomé et al. [169] showed evidence in documented AD cases that TDP-43 aggregates vary in their composition and relate to the clinical presentation. Here, our findings specifically demonstrate the importance of the

nature and number of NPs inhaled and swallowed. Hence, where you live, how you travel, what air pollutants you are exposed to, and your occupational history and exposure to any other environmental sources of NPs are as, if not more, important than all other factors known to be associated with neurodegeneration (CVD, diabetes, nutrition, exercise, etc.). The study has shortcomings. Our major gap is the lack of funding to extend the high resolution scanning and transmission electron microscopy (HRSTEM) and energy-dispersive X ray analysis (EDX).

4.2 Concluding Remarks

1. The neuropathological evidence from this new Mexico City study identifies unequivocal development of aberrant misfolding and aggregation of hyperphosphorylated tau, Aβ, α synuclein and TDP-43 in the brainstem of children and young adults.

2. Concentrations of Fe-rich, ferrimagnetic NPs in the brainstem vary from individual to individual, as expected for differing levels of NP exposure. Magnetic concentrations increasing in the order, SN < tectum/tegmentum/PAG < cerebellum, opens up the opportunity of detecting early clinical alterations in motor control learning, motor coordination, gait and balance [98], cognition and emotion behaviors and neurovegetative regulation.

3. Strikingly, we have identified, *in situ*, in SNpc neuronal organelles (mitochondria and neuromelanin), NPs containing Fe, Al and Ti in subjects displaying immunoreactive p-τ, αSyn and extensive NVU and mitochondrial damage. The elongate Ti-rich NPs in the SN, identical to Ti NPs in neuroenteric neurons are remarkable findings. Their presence strongly suggests that i.the GI tract is a key portal for Ti NPs, and ii. the oral portal of entry is a direct path to the brainstem via vagus nerves.

4. The portals of entry, and the specific characteristics (composition, size, etc.,) of the NPs may be of key importance in defining which cells and organelles will be affected and by what type of damage. The SN is an early target of metal-rich, and highly magnetic NPs: p-τ is the most common abnormal protein in young individuals.

5. The incursion of magnetite NPs from exogenous sources may not only induce neural ROS- and protein-related dysfunction. Given that magnetite formed biogenically by organisms can respond to small changes in magnetic field gradients and/or intensity (conferring a magnetoreceptive sense), it is possible that magnetite accumulated from exogenous sources can cause intra-cellular impacts through particle displacement/rotation, and by localised heating through microwave absorption.

6. Critical here are the co-associations between pathology seen in mitochondria, ER, and NM and the location and abundance of exogenous, Fe-, Al- and T-rich NPs, in close contact with key organelles and neurofilaments, glial fibers, and chromatin. Such reactive, cytotoxic and magnetic NPs are a specific potential source for all of the following: altered microtubule dynamics; mitochondrial dysfunction; accumulation and aggregation of unfolded proteins; abnormal endosomal systems; altered insulin signalling; altered calcium homeostasis; apoptotic signalling; autophagy; and epigenetic changes.

7. The bleak facts in sporadic PD is that the clinical motor manifestations are late [170, 171] with no possibility of reversing the extensive damage to dopaminergic cells, while in AD, the cognitive deficits develop very early and deeply compromise the potential academic, social and economic goals in young subjects.The TDP-43 pathology seen in 18% of young MMC urbanites obligate us to revise the dementia numbers in Mexico and Latin America (LA) and the prevalence of frontotemporal dementia (FTD).[172, 173, 162] Custodio et al. [172] discussed LA prevalence of dementia reaching 7.1%, with AD being the most frequent

type. FTD cases range from 12 to 18 cases per 1000 people with significant differences among Brazilians > Peruvians>Venezuelans. Mexico and LA are experiencing major demographic changes with increased numbers of people ≥60y and accurate prevalence data for AD and FTD in Mexico are both essential but presently not available.

8.These findings indicate that NP exposure shoud be included in any assessment of the neurodegenerative risk profile of each individual.

9. Highly oxidative, magnetic, abundant, metal-rich NPs emitted in the urban atmosphere constitute a novel path into AD, PD and TDP-43 pathogenesis. Exposed children and young adults need early neuroprotection and multidisciplinary prevention efforts have to be implemented. Control of combustion and friction nanoparticle sources (traffic, biomass burning, and industry), and of engineered NPs (food products, cosmetics, toothpaste, sun protectors, surface disinfectants, paints, e-waste etc) becomes increasingly important and urgent, in order to diminish the human and economic costs of a global neurodegenerative epidemic.

Acknowledgments

The authors thank Zabeada Aslam and Mark S'Ari of Leeds University's EPSRC Nanoscience and Nanotechnology Facility (LENNF), U.K. for their support and assistance in this work.

Author Contributions

Calderón-Garcidueñas Lilian: Conceptualization, data curation, formal analysis, Methodology, Investigation, Original draft preparation, Writing- Reviewing and Editing, Visualization, Supervision, Project administration. **Angélica González-Maciel, Rafael Reynoso-Robles, Randy Kulesza, Ingolf Lachmann, Ricardo Torres-Jardón, Partha S. Mukherjee:** Formal analysis, Visualization, Investigation, Supervision, Validation, Writing- Reviewing and Editing **Barbara Maher**: Data curation, formal analysis, writing-

reviewing and editing, visualization. SIRM, HRSTEM and EDX. HAADF-STEM images. **J. Hammond:** formal analysis, visualisation, investigation and validation.

Declaration of Competing Interest

The authors declare no competing financial interests. All data necessary to understand and assess the conclusions of this study are available in the main text. There are no restrictions on data availability in the manuscript.

1. Jung, C.R., Lin, Y.T., Hwang, B., 2015. Ozone, particulate matter, and newly diagnosed Alzheimer's disease: a population-based cohort study in Taiwan. J. Alzheimers Dis. 44, 573–584.

2. Chen, H., Kwong, J.C., Copes, R., et al., 2017. Living near major roads and the incidence of dementia, Parkinson's disease, and multiple sclerosis: a population-based cohort study. Lancet. 389, 718–726.

3. Lee, P.C., Liu, L.L., Sun, Y., et al., 2016. Traffic-related air pollution increased the risk of Parkinson's disease in Taiwan: A nationwide study. Environ Int. 96, 75-81. https://doi.org/10.1016/j.envint.2016.08.017.

4. Hu, C.Y., Fang, Y., Li, F.L., et al. 2019. Association between ambient air pollution and Parkinson's disease: Systematic review and meta-analysis. Environ Res. 168, 448-459. https://doi.org/10.1016/j.envres.2018.10.008.

5. Han, C., Lu, Y., Cheng, H., Wang, C., Chan, P., 2020. The impact of long-term exposure to ambient air pollution and second-hand smoke on the onset of Parkinson disease: a review and meta-analysis. Public Health. 179, 100-110. https://doi.org/10.1016/j.puhe.2019.09.020.

6. Calderón-Garcidueñas, L., Azzarelli, B., Acuna, H., et al., 2002. Air pollution and brain damage. Toxicol Pathol. 30, 373-389. https://doi.org/10.1080/01926230252929954.

7. Calderón-Garcidueñas, L., Maronpot, R.R., Torres-Jardon, R., et al., 2003. DNA damage in nasal and brain tissues of canines exposed to air pollutants is associated with evidence of chronic brain inflammation and neurodegeneration. Toxicol Pathol. 31,524-538. https://doi.org/10.1080/01926230390226645.

8. Calderón-Garcidueñas, L., Reed, W., Maronpot, R.R., et al., 2004. Brain inflammation and Alzheimer's-like pathology in individuals exposed to severe air pollution. Toxicol. Pathol. 32, 650-658. https://doi.org/10.1080/01926230490520232.

9. Calderón-Garcidueñas, L., Solt, A.C., Henríquez-Roldán, C., et al., 2008a. Long-term air pollution exposure is associated with neuroinflammation, an altered innate immune response, disruption of the blood-brain-barrier, ultrafine particulate deposition, and accumulation of amyloid beta-42 and alpha-synuclein in children and young adults. Toxicol. Pathol. 36, 289–310.

10. Calderón-Garcidueñas, L., Kavanaugh, M., Block, M., et al., 2012. Neuroinflammation, hyperphosphorylated tau, diffuse amyloid plaques, and down-regulation of the cellular prion protein in air pollution exposed children and young adults. J. Alzheimers. D. 28, 93-107

11. Calderón-Garcidueñas, L., Serrano-Sierra, A., Torres-Jardón, R., et al., 2013a. The impact of environmental metals in young urbanites' brains. Exp. Toxicol. Pathol. 65, 503-11.

12. Calderón-Garcidueñas, L., Franco-Lira, M., Mora-Tiscareño, A., et al., 2013b. Early Alzheimer's and Parkinson's disease pathology in urban children: Friend versus Foe responses-it is time to face the evidence. Biomed. Res. Int. 161687. https://doi.org/10.1155/2013/161687.

13. Calderón-Garcidueñas, L., González-González, L.O., Kulesza, R.J., Fech, T.M., et al., 2017a. Exposures to fine particulate matter ($PM_{2.5}$) and ozone above USA standards are associated with auditory brainstem dysmorphology and abnormal auditory brainstem evoked potentials in healthy young dogs. Environ. Res. 158, 324-332. https://doi.org/10.1016/j.envres.2017.06.026.

14. Calderón-Garcidueñas, L., Reynoso-Robles, R., Pérez-Guillé, B., et al., 2017b. Combustion derived nanoparticles, the neuroenteric system, cervical vagus, hyperphosphorilated alpha synuclein and tau in young Mexico City residents. Environ. Res. 159, 186–201.

15. Calderón-Garcidueñas, L., Gónzalez-Maciel, A., Reynoso-Robles, R., et al., 2018a. Hallmarks of Alzheimer disease are evolving relentlessly in Metropolitan Mexico City infants, children and young adults. APOE4 carriers have higher suicide risk and higher odds of reaching NFT stage V at ≤ 40 years of age. Environ. Res. 164, 475-487.

16. Calderón-Garcidueñas, L., González-Maciel, A., Reynoso-Robles, R., Kulesza, R.J., Mukherjee, P.S., Torres-Jardón, R., Rönkkö, T., Doty, R.L., 2018b. Alzheimer's disease and alpha-synuclein pathology in the olfactory bulbs of infants, children, teens and adults ≤ 40 years in Metropolitan Mexico City. APOE4 carriers at higher risk of suicide accelerate their olfactory bulb pathology. Environ. Res. 166, 348-362.

17. Calderón-Garcidueñas, L., González-Maciel, A., Mukherjee, P.S., Reynoso-Robles, R., Pérez-Guillé, B., Gayosso-Chávez, C., Torres-Jardón, R., Cross, J.V., Ahmed, I.A.M., Karloukovski, V.V., Maher, B.A., 2019a. Combustion- and friction-derived magnetic air

pollution nanoparticles in human hearts. Environ Res.176, 108567. https://doi.org/10.1016/j.envres.2019.108567

18. Calderón-Garcidueñas, L., Reynoso-Robles, R, González-Maciel, A., 2019b. Combustion and friction-derived nanoparticles and industrial-sourced nanoparticles: The culprit of Alzheimer and Parkinson's diseases. Environ. Res. 176, 108574. https://doi.org/10.1016/j.envres.2019.108574.

19. Calderón-Garcidueñas L, Kulesza, R.J., Mansour, Y., Aiello-Mora, M., Mukherjee, P.S., González-González, L.O., 2019c. Increased Gain in the Auditory Pathway, Alzheimer's Disease Continuum, and Air Pollution: Peripheral and Central Auditory System Dysfunction Evolves Across Pediatric and Adult Urbanites. J. Alzheimers. Dis. 70, 1275-1286. https://doi.org/10.3233/JAD-190405.

20. Calderón-Garcidueñas L, Torres-Jardón R, Kulesza RJ, Mansour Y, González-González LO, Gónzalez-Maciel A, Reynoso-Robles R, Mukherjee PS 2020a. Alzheimer disease starts in childhood in polluted Metropolitan Mexico City. A major health crisis in progress. Environ Res. 183:109137. https://doi: 10.1016/j.envres.2020.109137.

21. Calderón-Garcidueñas L, Herrera-Soto A, Jury N, Maher BA, González-Maciel A, Reynoso-Robles R, Ruiz-Rudolph P, van Zundert B, Varela-Nallar L. 2020b Reduced repressive epigenetic marks, increased DNA damage and Alzheimer's disease hallmarks in the brain of humans and mice exposed to particulate urban air pollution. Environ Res.183:109226. https://doi: 10.1016/j.envres.2020.109226.

22. Braak, H., Del Tredici, K., 2011. The pathological process underlying Alzheimer's disease in individuals under thirty. Acta. Neuropathol. 121, 171–181.

23. Braak, H., Del Tredeci, K., 2015. The preclinical phase of the pathological process underlying sporadic Alzheimer's disease. Brain. 138, 2814–2833.

24. Braak, H., Del Tredici, K., Rub, U., de Vos, R.A., Jansen Steur, E.N., Braak, E., 2003. Staging of brain pathology related to sporadic Parkinson's disease. Neurobiol. Aging. 24, 197–211.

25. Braak, H., Thal, D.R., Ghebremedhin, E., Del Tredeci, K., 2011. Stages of the pathological process in Alzheimer disease: age categories from 1 to 100 years. J. Neuropathol. Exp. Neurol. 70, 960–969.

26. Attems, J., Jellinger, K.A., 2006. Olfactory tau pathology in Alzheimer's disease and mild cognitive impairment. Clin. Neuropathol. 25, 265-271.

27. Attems, J., Walker, L., Jellinger, K.A., 2014. Olfactory bulb involvement in neurodegenerative diseases. Acta. Neuropathol.127, 459-75.

28. Thal, D.R., Rüb, U., Orantes, M., Braak, H., 2002. Phases of A beta-deposition in the human brain and its relevance for the development of AD. Neurology. 58, 1791-800. https://doi.org/10.1212/wnl.58.12.1791.

29. Rüb, U., Stratmann, K., Heinsen, H., et al., 2016. The brainstem tau cytoskeletal pathology of Alzheimer`s disease: A brief historical overview and description of its anatomical distribution pattern, evolutional features, pathogenetic and clinical relevance. Curr. Alzheimer. Res. 13, 1178-97. https://doi.org/10.2174/1567205013666160606100509.

30. Calderón-Garcidueñas, L., Franco-Lira, M., Henríquez-Roldán, C., et al., 2010. Urban air pollution: influences on olfactory function and pathology in exposed children and young adults. Exp. Toxicol. Pathol. 62, 91–102.

31. Calderón-Garcidueñas, L., D'Angiulli, A., Kulesza, R.J., et al., 2011a. Air pollution is associated with brainstem auditory nuclei pathology and delayed brainstem auditory evoked potentials. Int. J. Dev. Neurosci. 29, 365–375.

32. Calderón-Garcidueñas, L., Avila-Ramírez, J., Calderón-Garcidueñas, A., González-Heredia, T., et al., 2016a. Cerebrospinal Fluid Biomarkers in Highly Exposed PM2.5 Urbanites: The Risk of Alzheimer's and Parkinson's Diseases in Young Mexico City Residents. J. Alzheimers. Dis. 54, 597-613. https://doi.org/10.3233/JAD-160472.

33. Calderón-Garcidueñas, L., Reynoso-Robles, R., Vargas-Martínez, J., et al., 2016b. Prefrontal white matter pathology in air pollution exposed Mexico City young urbanites and their potential impact on neurovascular unit dysfunction and the development of Alzheimer's disease. Environ. Res. 146, 404-417. https://doi.org/10.1016/j.envres.2015.12.031.

34. Mansour, Y., Blackburn, K., González-González, L.O., Calderón-Garcidueñas, L., Kulesza, R.J., 2019. Auditory brainstem dysfunction,non-invasive biomarkers for early diagnosis and monitoring of Alzheimer's disease in young urban residents exposed to air pollution. J. Alzheimers. Dis. 67, 1147-1155. https://doi.org/10.3233/JAD-181186.

35. Jack, C.R. Jr., Bennett, D.A., Blennow, K., et al., 2018. NIA-AA Research Framework: Toward a biological definition of Alzheimer's disease. Alzheimers Dement. 14, 535-562. https://doi.org/10.1016/j.jalz.2018.02.018.

36. Jack, C.R.Jr., Therneau, T.M.,Weigand, S.D., et al., 2019. Prevalence of Biologically vs Clinically Defined Alzheimer Spectrum Entities Using the National Institute on Aging-Alzheimer's Association Research Framework. JAMA Neurol. 76, 1174-1183. httpss://doi.org/10.1001/jamaneurol.2019.1971.

37. Maher, B., Ahmed, I.A.M., Karloukovski, V., et al. 2016. Magnetite pollution nanoparticles in the human brain. Proc. Natl. Acad.Sci, USA.113, 10797-10801. https://doi.org/10.1073/pnas.1605941113.

38. González-Maciel, A., Reynoso-Robles, R., Torres-Jardón, R., et al., 2017. Combustion derived nanoparticles in key brain target cells and organelles in young urbanites: culprit hidden in plain sight in Alzheimer's disease development. J. Alzheimers. Dis. 59, 189–208.

39. Maher, B. A., González-Maciel, A., Reynoso-Robles, R., Torres-Jardón, R., Calderón-Garcidueñas, L., 2020. Iron-rich air pollution nanoparticles: An unrecognised environmental risk factor for myocardial mitochondrial dysfunction and cardiac oxidative stress. Environ. Res. 188, 109816. https://doi.org/10.1016/j.envres.2020.109816

40. Maher, B.A., 2019. Airborne Magnetite- and Iron-Rich Pollution Nanoparticles: Potential Neurotoxicants and Environmental Risk Factors for Neurodegenerative Disease, Including Alzheimer's Disease. J. Alzheimers. Dis. 71, 361-375. https://doi.org/10.3233/JAD-190204.

41. Gonet, T., Maher, B.A., 2019. Airborne, Vehicle-Derived Fe-Bearing Nanoparticles in the Urban Environment: A Review. Environ Sci Technol. 53, 9970-9991. https://doi.org/10.1021/acs.est.9b01505.

42. Villalobos-Pietrini, R., Amador-Muñoz, O., Valle-Hernández, B., Gómez-Arroyo, S., Waliszewski, S., Jazcilevich, A.D., 2011. Organic Compound in Airborne Particles and their Genotoxic Effects in Mexico City, In: Air Quality Monitoring, Assessment and Management. (Nicolás A. Mazzeo). IntechOpen. pp. 345-378

43. Rowangould GM. 2013. A census of the US near-roadway population: Public health and environmental justice considerations. Transportation Research Part D: Transport and Environment 25;59-67

44. Su, J.G., Apte, J.S., Lipsitt, J., et al., 2015. Populations potentially exposed to traffic-related air pollution in seven world cities. Environ Int. 78, 82-89. https://doi-org/10.1016/j.envint.2014.12.007.

45. Ladino, L.A., Raga, G.B., Baumgardner, D., 2018. On particle-bound polycyclic aromatic hydrocarbons (PPAH) and links to gaseous emissions in Mexico City. Atmospheric. Environment. 194, 31-40.

46. Delfino, R. J., Sioutas, C., Malik, S., 2005. Potential role of ultrafine particles in associations between airborne particle mass and cardiovascular health. Environ. Health. Perspect. 113, 934-946. https://doi.org/10.1289/ehp.7938.

47. Solaimani, P., Saffari, A., Sioutas, C., Bondy, S.C., Campbell, A., 2017. Exposure to ambient ultrafine particulate matter alters the expression of genes in primary human neurons. Neurotoxicology. 58, 50-57. https://doi.org/10.1016/j.neuro.2016.11.001.

48. Weichenthal, S., Olaniyan, T., Christidis, T., et al., 2020. Within-city spatial variations in ambient ultrafine particle concentrations and incident brain tumors in adults. Epidemiology. 31, 177-183. https://doi.org/10.1097/EDE.0000000000001137

49.Brostøm A, Kling KI, Koponen IK, Hougaard KS, Kandler K, Mølhave K. 2019. Improving the foundation for particulate matter risk assessment by individual nanoparticle statistics from electron microscopy analysis**.** Sci Rep 9:8093 doi: 10.1038/s41598-019-44495-7.

50.Boyes WK, van Thriel C. 2020.Neurotoxicology of Nanomaterials. Chem Res Toxicol 33:1121-1144

51.Ceballos D, Zhou M, Herrick R. Metals and Particulates Exposure from a Mobile E-Waste Shredding Truck: A Pilot Study. 2020. Ann Work Expo Health Aug 4; wxaa058 doi: 10.1093/annweh/wxaa058

52.Caudillo L, Salcedo D, Peralta O, Castro T, Alvarez-Ospina H. 2020. Nanoparticle size distributions in Mexico City. Atmospheric Pollution Research. 1:78-84

53. Linse, S., Cabaleiro-Lago, C., Xue, W.F., 2007. Nucleation of protein fibrillation by nanoparticles. Proc. Natl. Acad. Sci. USA. 104, 8691-8696.

54. Kumari, M., Rajak, S., Singh, S.P., et al., 2012. Repeated oral dose toxicity of iron oxide nanoparticles: biochemical and histopathological alterations in different tissues of rats. J. Nanosci. Nanotechnol. 12, 2149-2159

55. Yarjanli, Z., Ghaedi, K., Esmaeili, A., Rahgozar, S., Zarrabi, A., 2017. Iron Oxide Nanoparticles May Damage to the Neural Tissue Through Iron Accumulation, Oxidative Stress, and Protein Aggregation. BMC Neurosci. 18, 51. https://doi.org/10.1186/s12868-017-0369-9.

56. Saptarshi, S.R., Duschl, A., Lopata, A.L., 2013. Interaction of nanoparticles with proteins: relation to bio-reactivity of the nanoparticle. J. Nanobiotech. 11, 26. https://doi.org/10.1186/1477-3155-11-26.

57. Parveen, R., Shamsi, T.N., Fatima, S., 2017. Nanoparticles-protein interaction: Role in protein aggregation and clinical implications. Int. J. Biol. Macromol. 94, 386-395. https:// doi.org/10.1016/j.ijbiomac.2016.10.024.

58. Pacakova, B., Kubickova, S., Salas, G., et al., 2017. The internal structure of magnetic nanoparticles determines the magnetic response. Nanoscale. 9, 5129-5140. https://doi.org/10.1039/c6nr07262c.

59. Gutiérrez, L., de la Cueva, L., Moros, M., et al., 2019. Aggregation effects on the magnetic properties of iron oxide colloids. Nanotechnology. 30, 112001. https://doi.org/10.1088/1361-6528/aafbff.

60. Imam, S.Z., Lantz-McPeak, S.M., Cuevas, E., et al., 2015. Iron Oxide Nanoparticles Induce Dopaminergic Damage: In vitro Pathways and In Vivo Imaging Reveals Mechanism of Neuronal Damage. Mol Neurobiol. 52, 913-926. https://doi.org/10.1007/s12035-015-9259-2.

61. Kim, Y., Ko, S.M., Nam, J.M., 2016. Protein-Nanoparticle Interaction-Induced Changes in Protein Structure and Aggregation. Chem Asian J. 11, 1869-1877. https://doi.org/10.1002/asia.201600236

62. Hartl, F.U., 2017. Protein Misfolding Diseases. Annu Rev Biochem. 86, 21-26. https://doi.org/10.1146/annurev-biochem-061516-044518.

63. Chandel, T.I., Zaman, M., Khan, M.V., et al., 2018. A mechanistic insight into protein-ligand interaction, folding, misfolding, aggregation and inhibition of protein aggregates: An overview. Int. J. Biol. Macromol. 106, 1115-1129.

64. Venkatraman, A., Edlow, B.L., Immordino-Yang, M.H., 2017. The Brainstem in Emotion: A Review. Front. Neuroanat. 11,15. https://doi.org/ 10.3389/fnana.2017.00015.

65. Zhang, Y., Larcher, K.M., Misic, B., Dagher, A., 2017. Anatomical and functional organization of the human substantia nigra and its connections. Elife. 6, e26653. https://doi.org/10.7554/eLife.26653

66. Zelena, D., Menant, O., Andersson, F., Chaillou, E., 2018. Periaqueductal gray and emotions: the complexity of the problem and the light at the end of the tunnel, the magnetic resonance imaging. Endocr Regul. 52, 222-238. https://doi.org/10.2478/enr-2018-0027.

67. Adamaszek, M., D'Agata, F., Ferrucci, R., Habas, C., et al., 2017. Consensus Paper: Cerebellum and Emotion. Cerebellum. 16, 552-576. https://doi.org/10.1007/s12311-016-0815-8.

68. Molina, L.T., Madronich, S., Gaffney, J.S., et al., 2010. An overview of the MILAGRO 2006 Campaign: Mexico City emissions and their transport and transformation. Atmos. Chem. Phys. 10, 8697–8760. https://doi.org/10.5194/acp-10-8697-2010, 2010.

69. Molina, L.T., Velasco, E., Retama, A., Zavala, M., 2019. Experience from Integrated Air Quality Management in the Mexico City Metropolitan Area and Singapore. Atmosphere. 10, 512

70. Guerrero, F., Alvarez-Ospina, H., Retama, A., et al., 2017. Seasonal changes in the PM 1 chemical composition north of Mexico City. Atmósfera. 30, 243-258.

71. Dzepina, K., Arey, J., Marr, L.C., et al., 2007. Detection of particle-phase polycyclic aromatic hydrocarbons in Mexico City using an aerosol mass spectrometer. Int. J. Mass Spectrom. 263, 152–170.

72. Querol, X., Pey, J., Minguillón, M.C., et al., 2008. PM speciation and sources in Mexico during the MILAGRO-2006 Campaign. Atmos. Chem. Phys. 8, 111-128. https://doi.org/10.5194/acp-8-111-2008, 2008.

73. Velasco, E., Retama, A., 2017. Ozone's threat hits back Mexico City. Sustainable Cities and Society. 31, 260-263. https://doi.org/10.1016/j.scs.2016.12.015.

74. Torres-Jardón, R., 2018. Políticas públicas y su efecto en la calidad del aire de la Zona Metropolitana de la Ciudad de México. In: Transversalidad de la Política del Aire en México. (Sosa Núñez, G. S.), Instituto de Investigaciones Dr. José María Luis Mora. México, D. F., pp. 43-74.

75. Verma, V., Shafer, M. M., Schauer, J. J., Sioutas, C., 2010. Contribution of transition metals in the reactive oxygen species activity of PM emissions from retrofitted heavy-duty vehicles. Atmos. Environ. 44, 5165-5173.

76. Maher, B. A., Ahmed, I. A., Davison, B., Karloukovski, V., Clarke, R., 2013. Impact of roadside tree lines on indoor concentrations of traffic-derived particulate matter. Environ. Sci. Technol. 47, 13737–13744. https://doi.org/10.1021/es404363m.

77. Sanderson, P., Su, S.S., Chang, I.T.H., Delgado Saborit, J.M., et al., 2016. Characterisation of iron-rich atmospheric submicrometre particles in the roadside environment. Atmos. Environ. 140, 167-175. https://doi.org/10.1016/j.atmosenv.2016.05.040.

78. Adachi, K., Buseck, P.R., 2010. Hosted and free-floating metal-bearing atmospheric nanoparticles in Mexico City. Environ. Sci. Technol. 44, 2299-2304. https://doi.org/10.1021/es902505b.

79. Braak, H., Del Tredici, K., 2017. Neuropathological Staging of Brain Pathology in Sporadic Parkinson's disease: Separating the Wheat from the Chaff. J. Parkinsons. Dis. 7, S73-S87.

80. Braak, H., Del Tredici, K., 2018. Anterior Cingulate Cortex TDP-43 Pathology in Sporadic Amyotrophic Lateral Sclerosis. J. Neuropathol. Exp. Neurol. 77, 74-83

81. Del Tredici, K., Rüb, U., De Vos, R.A., et al., 2002. Where does Parkinson disease pathology begin in the brain? J. Neuropathol. Exp. Neurol. 61,413-26.8

82. Del Tredici, K., Braak, H., 2016. Review: Sporadic Parkinson's disease: development and distribution of α-synuclein pathology. Neuropathol. Appl. Neurobiol. 42, 33-50. https://doi.org/10.1111/nan.12298

83. Beach,T.G., White, C.L.III., Hladik, C.L., et al., 2009. Olfactory bulb alpha-synucleinopathy has high specificity and sensitivity for Lewy body disorders. Acta. Neuropathol. 117, 169–174.

84. Tsuboi, Y., Wszolek, Z.K., Graff-Radford, N.R., et al., 2003. Tau pathology in the olfactory bulb correlates with Braak stage, Lewy body pathology and apolipoprotein epsilon4. Neuropathol. Appl. Neurobiol. 29, 503-10. https:// doi.org/10.1046/j.1365-2990.2003. 00453. X

85. McKeith, I.G., Dickson, D.W., Lowe, J., et al., 2005. Diagnosis and management of dementia with Lewy bodies: third report of the DLB Consortium. Neurology. 65, 1863-1872. https://doi:10.1212/01.wnl.0000187889.17253.b1.

86. Brettschneider, J., Del Tredici, K., Toledo, J.B., et al., 2013. Stages of pTDP-43 pathology in amyotrophic lateral sclerosis. Ann. Neurol. 74, 20-38.

87. Shahmoradian, S.H., Lewis, A.J., Genoud, C., et al., 2019. Lewy pathology in Parkinson's disease consists of crowded organelles and lipid membranes. Nat Neurosci. 22, 1099-1109. https://doi.org/10.1038/s41593-019-0423-2.

88. Maher, B.A., 1988, Magnetic properties of some synthetic sub- micron magnetites. Geophys. J. Roy. Astr. Soc. 94, 83-96. https://doi.org/10.1111/j.1365-246X.1988.tb03429.x

89. Dewey, C.M., Cenik, B., Sephton, C.F., et al., 2012. TDP-43 aggregation in neurodegeneration: are stress granules the key?. Brain Res. 1462, 16-25. https://doi.org/10.1016/j.brainres.2012.02.032

90. James, B. D., Wilson, R. S., Boyle, P. A., Trojanowski, J. Q., Bennett, D. A., Schneider, J. A., 2016. TDP-43 stage, mixed pathologies, and clinical Alzheimer's-type dementia. Brain. 139, 2983–2993. https://doi.org/10.1093/brain/aww224.

91. Nelson, P.T., Dickson, D.W., Trojanowski, J.Q., et al., 2019. Limbic-predominant age-related TDP-43 encephalopathy (LATE): consensus working group report. Brain. 142, 1503-1527. https://doi.org/10.1093/brain/awz099.

92. Kodavati, M., Wang, H., Hegde, M.L., 2020. Altered Mitochondrial Dynamics in Motor Neuron Disease: An Emerging Perspective. Cells. 9,1065. https://doi.org/10.3390/cells9041065.

93. Besnard-Guérin, C., 2020. Cytoplasmic Localization of Amyotrophic Lateral Sclerosis-Related TDP-43 Proteins Modulates Stress Granule Formation. Eur. J. Neurosci. https://doi.org/10.1111/ejn.14762.

94. Pasquini, L., Nana, A.L., Toller, G., et al., 2020. Salience Network Atrophy Links Neuron Type-Specific Pathobiology to Loss of Empathy in Frontotemporal Dementia. Cereb. Cortex. 119. https://doi.org/10.1093/cercor/bhaa119.

95. Wu, C.C., Jin, L.W., Wang, I.F., et al., 2020. HDAC1 dysregulation induces aberrant cell cycle and DNA damage in progress of TDP-43 proteinopathies. EMBO Mol. Med. 12, e10622. https://doi.org/10.15252/emmm.201910622.

96. Mashiko T, Sakashita E, Kasashima K, Tominaga K, Kuroiwa K, Nozaki Y, Matsuura T, Hamamoto T, Endo H.J 2016. Developmentally Regulated RNA-binding Protein 1 (Drb1)/RNA-binding Motif Protein 45 (RBM45), a Nuclear-Cytoplasmic Trafficking Protein, Forms TAR DNA-binding Protein 43 (TDP-43)-mediated Cytoplasmic Aggregates. Biol Chem. 291(29):14996-5007.

97. Guyenet, P. G., Stornetta, R. L., Souza, G.M.P.R., Abbott, S.B.G., Brooks, V. L., 2020. Neuronal Networks in Hypertension: Recent Advances. Hypertension. 2020, HYPERTENSIONAHA12014521. https://doi.org/10.1161/HYPERTENSIONAHA.120.14521

98. Calderón-Garcidueñas L, Ana Karen Torres-Solorio AK, Kulesza RJ, Torres-Jardón R, González-González LO, García-Arreola B, Chávez-Franco DA, Luévano-Castro SC, Hernández-Castillo A, Carlos-Hernández E, Solorio-López E, Crespo-Cortés CN, Research Universidad del Valle de México UVM Group, Partha S. Mukherjee.2020c.Gait and balance disturbances are common in young urbanites and associated with cognitive impairment. Air pollution and the historical development of Alzheimer's disease in the young.

99. Chemseddine, A., Moritz, T., 1999. Nanostructuring Titania: Control over nanocrystal structure, size, shape, and organization. Eur. J. Inorg. Chem. 1999, 235-245. https://doi.org/10.1002/(SICI)1099-0682(19990202)1999:2<235::AID-EJIC235>3.0.CO;2-N

100. Chen, X., Mao, S.S., 2007. Titanium dioxide nanomaterials: synthesis, properties, modifications, and applications. Chem Rev. 107,2891-2959. https://doi.org/10.1021/cr0500535.

101. Kose O, Tomatis M, Leclerc L, Belblidia NB, Hochepied JF, Turci F, Pourchez J, Forest V. 2020. Impact of the physicochemical features of TiO2 nanoparticles on their in vitro toxicity.Chem Res Toxicol. doi: 10.1021/acs.chemrestox.0c00106

102. Lu, D., Luo, Q., Chen, R., Zhuansun, Y., Jiang, J., Wang, W., et al., 2020. Chemical multi-fingerprinting of exogenous ultrafine particles in human serum and pleural effusion. Nat. Commun. 11, 2567. https://doi.org/10.1038/s41467-020-16427-x.

103. Holmqvist, S., Chutna, O., Bousset, L., et al., 2014. Direct evidence of Parkinson pathology spread from the gastrointestinal tract to the brain in rats. Acta Neuropathol. 128, 805-820. https://doi.org/10.1007/s00401-014-1343-6.

104. Anselmi, L., Toti, L., Bove, C., Hampton, J., Travagli, R.A., 2017a. A nigro vagal pathway controls gastric motility and is affected in a rat model of

Parkinsonism. Gastroenterology. 153, 1581-1593. https://doi-org/:10.1053/j.gastro.2017.08.069.

105. Anselmi, L., Toti, L., Bove, C., Travagli, R.A., 2017b. Vagally mediated effects of brain stem dopamine on gastric tone and phasic contractions of the rat. Am. J. Physiol Gastrointest. Liver. Physiol. 313, G434-G441. https://doi.org/10.1152/ajpgi.00180.2017

106. Arshadi M, Yaghmei S, Mohammed Mousavi S.Analysis on characteristics of different kinds of e waste.Proceedings Sardinia 2017 / Sixteenth International Waste Management and Landfill Symposium/ 2 - 6 October 2017 S. Margherita di Pula, Cagliari, Italy / © 2017 by CISA Publisher, Italy

107. Sungur, Ş., Kaya, P., Koroglu, M., 2020. Determination of Titanium Dioxide Nanoparticles Used in Various Foods. Food. Addit. Contam. 1-8. https://doi.org/10.1080/19393210.2020.1769193.

108. Xu, S., Sui, J., Fu, Y., et al., 2020. Titanium dioxide nanoparticles Induced the Apoptosis of RAW264.7 Macrophages Through miR-29b-3p/NFAT5 Pathway. Environ. Sci. Pollut. Res Int. 2020;10.1007/s11356-020-08952-5. https://doi.org/10.1007/s11356-020-08952-5.

109. Yao, L., Tang, Y., Chen, B., et al., 2020. Oral Exposure of Titanium Oxide Nanoparticles Induce Ileum Physical Barrier Dysfunction via Th1/Th2 Imbalance. Environ. Toxicol. 2020;10.1002/tox.22934. https://doi.org/10.1002/tox.22934.

110. Peters RJB, Oomen AG, van Bemmel G, et al., 2020. Silicon dioxide and titanium dioxide particles found in human tissues.Nanotoxicology.14(3):420-432. https://doi: 10.1080/17435390.2020.1718232.

111. Coméra C, Cartier C, Gaultier E et al., 2020. Jejunal Villus Absorption and Paracellular Tight Junction Permeability Are Major Routes for Early Intestinal Uptake of Food-Grade TiO $_2$ Particles: An in Vivo and Ex Vivo Study in Mice**.**Part Fibre Toxicol June 11; 17(1):26. doi: 10.1186/s12989-020-00357-z.

112. Gallocchio F, Biancotto G, Moressa A et al., 2020. Bioaccumulation and in Vivo Formation of Titanium Dioxide Nanoparticles in Edible Mussels.Food Chem 323:126841 doi: 10.1016/j.foodchem.2020.126841.

113. Tiwary CS, Kishore S, Vasireddi R, Mahapatra DR, Ajayan PM, Chattopadhyay K.2017. Electronic waste recycling via cryo-milling and nanoparticle beneficiation.Materials Today 20:67-73 https://doi.org/10.1016/j.mattod.2017.01.015

114. Gilder SA, Wack M, Kaub L et al., 2018. Distribution of Magnetic Remanence Carriers in the Human Brain**.**Sci Rep 8(1):11363 doi: 10.1038/s41598-018-29766-z.

115. Wang, S., Zhang, B., Su, L., et al., 2019. Subcellular Distributions of Iron Oxide Nanoparticles in Rat Brains Affected by Different Surface Modifications. J. Biomed. Mater. Res A. 107, 1988-1998. https;//doi.org/10.1002/jbm.a.36711.

116. Bergamino, M., Keeling, E.G. , Mishra, V.R., Stokes, A.M., Walsh, R.R., 2020. Assessing white matter pathology in early-stage Parkinson Disease using diffusion MRI: A Systematic Review. Front. Neurol. 11, 314. https://doi.org/10.3389/fneur.2020.00314.

117. Liu, Y., Li, J., Xu, K., et al., 2018. Characterization of Superparamagnetic Iron Oxide Nanoparticle-Induced Apoptosis in PC12 Cells and Mouse Hippocampus and Striatum. Toxicol. Lett. 292, 151-161. https://doi.org/10.1016/j.toxlet.2018.04.033.

118. Mohammadi, S., Nikkhah, M., 2017. TiO2 Nanoparticles as Potential Promoting Agents of Fibrillation of α-Synuclein, a Parkinson's Disease-Related Protein. Iran. J. Biotechnol. 15, 87-94. https://doi.org/10.15171/ijb.1519.

119. Milatovic, D., Zaja-Milatovic, S., Gupta, R.C., Yu, Y., Aschner, M., 2009. Oxidative damage and neurodegeneration in manganese-induced neurotoxicity. Toxicol. Appl. Pharmacol. 240, 219-225. https://doi.org/10.1016/j.taap.2009.07.004.

120. Tahaei Gilan, S.S., Yahya Rayat, D., Mustafa, T.A., et al., 2019. α-synuclein interaction with zero-valent iron nanoparticles accelerates structural rearrangement into amyloid-susceptible structure with increased cytotoxic tendency. Int. J. Nanomedicine. 14, 4637-4648. https://doi.org/10.2147/IJN.S212387.

121. Tira, R., De Cecco, E., Rigamonti, V., et al., 2020. Dynamic molecular exchange and conformational transitions of alpha-synuclein at the nano-bio interface. Int. J. Biol. Macromol. 154, 206-216. https://doi.org/10.1016/j.ijbiomac.2020.03.118.

122. Chen Y, Landin-Romero R, Kumfor F, Irish M, Hodges JR, Piguet O. 2020. Cerebellar structural connectivity and contributions to cognition in frontotemporal dementias. Cortex.129:57-67. doi: 10.1016/j.cortex.2020.04.013.

123. Gupta, G., Gliga, A., Hedberg, J., et al., 2020. Cobalt Nanoparticles Trigger Ferroptosis-Like Cell Death (Oxytosis) in Neuronal Cells: Potential Implications for Neurodegenerative Disease. FASEB J. 34, 5262-5281. https://doi.org/10.1096/fj.201902191RR.

124. Reddy, U.A., Prabhakar, P.V., Mahboob, M., 2017. Biomarkers of oxidative stress for *in vivo* assessment of toxicological effects of iron oxide nanoparticles. Saudi. J. Biol. Sci. 24, 1172-1180. https://doi.org/10.1016/j.sjbs.2015.09.029.

125. Wu, T., Tang, M., 2018. The inflammatory response to silver and titanium dioxide nanoparticles in the central nervous system. Nanomedicine. 13, 233-249. https://doi.org/10.2217/nnm-2017-0270.

126. Disdier, C., Chalansonnet, M., Gagnaire, F., Gaté, L., et al., 2017. Brain inflammation, blood brain barrier dysfunction and neuronal synaptophysin decrease after inhalation exposure to Titanium Dioxid nano-aerosol in aging rats. Sci Rep. 7, 12196. https://doi.org/10.1038/s41598-017-12404-5.

127. Berndt, D., Millward, J.M., Schnorr, J., Taupitz, M., et al., 2017. Inflammation-induced brain endothelial activation leads to uptake of electrostatically stabilized iron oxide nanoparticles via sulfated glycosaminoglycans. Nanomedicine. 13, 1411-1421.

128. Ehsanifar, M., Tameh, A.A., Farzadkia, M., et al., 2019.Exposure to nanoscale diesel exhaust particles: Oxidative stress, neuroinflammation, anxiety and depression on adult male mice. Ecotoxicol. Environ. Saf. 168, 338-347.

129. Ising, C., Venegas, C.,Zhang, S., et al., 2019. NLRP3 inflammasome activation drives tau pathology. Nature. 575, 669-673. https://doi.org/10.1038/s41586-019-1769-z.

130. Teller S, Tahirbegi IB, Mir M, Samitier J, Soriano J. 2015. Magnetite-Amyloid-β deteriorates activity and functional organization in an in vitro model for Alzheimer's disease.Sci Rep. 5:17261. doi: 10.1038/srep17261.

131. Quintana C, Bellefqih S, Laval JY et al., 2006. Study of the localization of iron, ferritin, and hemosiderin in Alzheimer's disease hippocampus by analytical microscopy at the subcellular level.Struct Biol.153(1):42-54. doi: 10.1016/j.jsb.2005.11.001.

132. Castellani, R.J., Moreira, P.I., Liu, G., et al., 2007. Iron: the Redox-active center of oxidative stress in Alzheimer disease. Neurochem Res. 32, 1640-1645. https://doi.org/10.1007/s11064-007-9360-7.

133. Allsop, D., Mayes, J., Moore, S., Masad, A., Tabner, B. J., 2008. Metal-dependent generation of reactive oxygen species from amyloid proteins implicated in neurodegenerative disease. Biochemical. Society. Transactions. 36, 1293–1298. https://doi.org/10.1042/BST0361293.

134. Coccini, T., Caloni, F., Ramírez Cando, L.J., De Simone, U., 2017. Cytotoxicity and proliferative capacity impairment induced on human brain cell cultures after short- and long-term exposure to magnetite nanoparticles. J. Appl. Toxicol. 37, 361-373. https://doi.org/10.1002/jat.3367.

135. Kirschvink, J. L., Kobayashi-Kirschvink, A., Diaz-Ricci, J. C., Kirschvink, S. J., 1992. Magnetite in human tissues: a mechanism for the biological effects of weak ELF magnetic fields. Bioelectromagnetics. 1, 101–113. https://doi.org/10.1002/bem.2250130710

136.Pall ML. 2018. Wi-Fi is an important threat to human health. Environ Res 164:405-416

137.Karimi A, Moghaddam FG, Valipour M.2020. Insights in the biology of extremely low-frequency magnetic fields exposure on human health. Mol Biol Rep 47:5621-5633

138.Gholami A, Mousavi SM, Hashemi SA, Ghasemi Y, Chiang WH, Parvin N.2020. Current trends in chemical modifications of magnetic nanoparticles for targeted drug delivery in cancer chemotherapy. Drug Metab Rev 52:205-224

139. Kirschvink, J. L., and Gould, J. L., 1981, Biogenic magnetite as a basis for magnetic field sensitivity in animals, *BioSystems* **13**: 181–201.

140. Binhi, V.N., Prato, F.S., 2018. Rotations of macromolecules affect nonspecific biological responses to magnetic fields. Sci. Rep. 8, 13495. https://doi.org/10.1038/s41598-018-31847-y.

141. Falone, S., Santini, S.Jr., Cordone, V., et al., 2018. Extremely Low-Frequency Magnetic Fields and Redox-Responsive Pathways Linked to Cancer Drug Resistance: Insights from Co-Exposure-Based *In Vitro* Studies. Front. Public Health, 6, 33. https://doi.org/10.3389/fpubh.2018.00033.

142. Casey, J.S., Arrizabalaga, J.H., Abu-Laban, M., et al., 2020. Alternating Magnetic Field Mediated Release of Fluorophores from Magnetic Nanoparticles by Hysteretic Heating. J. Colloid. Interface. Sci. 571, 348-355. https://doi.org/10.1016/j.jcis.2020.03.056.

143. Gao, H., Zhang, T., Zhang, Y., et al., 2020. Ellipsoidal Magnetite Nanoparticles: A new member of the magnetic-vortex nanoparticles family for efficient magnetic hyperthermia. J. Mater. Chem B. 8, 515-522. https://doi.org/10.1039/c9tb00998a.

144. Afitska, K., Fucikova, A., Shvadchak, V.V., Yushchenko, D.A., 2019. α-Synuclein aggregation at low concentrations**.** Biochim. Biophys. Acta. Proteins. Proteom. 1867, 701-709. https://doi.org/10.1016/j.bbapap.2019.05.003.

145. Virk, S.A., Eslick, G.D., 2015. Brief Report: Meta-analysis of antacid use and Alzheimer's disease: Implications for the aluminum hypothesis. Epidemiology. 26, 769-773. https://doi.org/10.1097/EDE.0000000000000326.

146. Perl, D.P., Brody, A.R. 1980. Alzheimer's Disease: X-ray Spectrometric Evidence of Aluminum Accumulation in Neurofibrillary Tangle-Bearing Neurons**.**Science 208(4441):297-299 doi: 10.1126/science.7367858.

147. Perl, D.P., Good, P.F., 1987. Uptake of aluminium into central nervous system along nasal-olfactory pathways. Lancet. 1, 1028. https://doi.org/10.1016/s0140-6736(87)92288-4

148. Hashimoto, M., Imazato, S., 2015. Cytotoxic and genotoxic characterization of aluminium and silicon oxide nanoparticles in macrophages. Dent. Mater. 31, 556–564. https://doi.org/10.1016/j.dental.2015.02.009.

149. Shang, N., Zhang, P., Wang, S., et al., 2020. Aluminum-Induced Cognitive Impairment and PI3K/Akt/mTOR signaling pathway involvement in occupational aluminum workers. Neurotox. Res. 2020,10.1007/s12640-020-00230-z. https://doi.org/10.1007/s12640-020-00230-z.

150. Exley, C., Clarkson, E., 2020. Aluminium in human brain tissue from donors without neurodegenerative disease: A comparison with Alzheimer's disease, multiple sclerosis and autism. Sci. Rep. 10, 7770. https://doi.org/10.1038/s41598-020-64734-6.

151. Haining, R.L, Achat-Mendes, C., 2017. Neuromelanin, one of the most overlooked molecules in modern medicine, is not a spectator. Neural Regen Res. 12, 372–375. https://doi.org/10.4103/1673-5374.202928: 10.4103/1673-5374.202928

152. Zecca L, Bellei C, Costi P, et al., 2008. New melanic pigments in the human brain that accumulate in aging and block environmental toxic metals. Proc Natl Acad Sci U S A. 105(45):17567-17572. https://doi: 10.1073/pnas.0808768105.

153. Zucca, F.A., Vanna, R., Cupaioli, F.A., et al., 2018. Neuromelanin organelles are specialized autolysosomes that accumulate undegraded proteins and lipids in aging human brain and are likely involved in Parkinson's disease**.** NPJ. Parkinsons. Dis. 4, 17. https://doi.org/10.1038/s41531-018-0050-8.

154. Limanaqi, F., Biagioni, F., Gambardella, S., et al., 2020. Promiscuous Roles of Autophagy and Proteasome in Neurodegenerative Proteinopathies. Int. J. Mol. Sci. 21, 3028. https://doi.org/10.3390/ijms21083028.

155. George S, Rey NL, Tyson T, et al., 2019. Microglia Affect α-synuclein Cell-To-Cell Transfer in a Mouse Model of Parkinson's Disease.Mol Neurodegener 14:34. https://doi: 10.1186/s13024-019-0335-3.

156. Li H, Chen Z, Li J, Liu R, Zhao F, Liu R. 2020. Indium Oxide Nanoparticles Induce Lung Intercellular Toxicity Between Bronchial Epithelial Cells and Macrophages.J Appl Toxicol https://doi: 10.1002/jat.4023

157. Vanella, K.M., Wynn, T.A. 2017. Mechanisms of Organ Injury and Repair by Macrophages.Annu Rev Physio 79:593-617

158. Wang TS, Coppens I, Saorin A, Brady NR, Hamacher-Brady A. 2020. Endolysosomal Targeting of Mitochondria Is Integral to BAX-Mediated Mitochondrial Permeabilization During Apoptosis Signaling.Dev Cell 53(6):627-645.e7. doi: 10.1016/j.devcel.2020.05.014

159. Moore, S., Rabichow, B.E., Sattler, R., 2020. The Hitchhiker's Guide to Nucleocytoplasmic Trafficking in Neurodegeneration. Neurochem. Res. 45, 1306-1327. https://doi.org/10.1007/s11064-020-02989-1.

160. Leibiger, C., Deisel, J., Aufschnaiter, A., et al. 2018. TDP-43 Controls Lysosomal Pathways Thereby Determining Its own clearance and cytotoxicity. Hum. Mol. Genet. 27, 1593-1607. https://doi.org/10.1093/hmg/ddy066.

161. Koren, S.A., Galvis-Escobar, S., Abisambra. J.F., 2020. Tau-mediated Dysregulation of RNA: Evidence for a Common Molecular Mechanism of Toxicity in Frontotemporal

Dementia and Other Tauopathies. Neurobiol. Dis. 141, 104939. https://doi.org/10.1016/j.nbd.2020.104939.

162. Advani, V.M., Ivanov, P., 2020. Stress Granule Subtypes: An Emerging Link to Neurodegeneration. Cell. Mol. Life. Sci. https://doi.org/10.1007/s00018-020-03565-0.

163. Pierce, J.E., Péron, J. 2020. The Basal Ganglia and the Cerebellum in Human Emotion. Soc Cogn Affect Neurosci 15(5):599-613. doi: 10.1093/scan/nsaa076.

164. Tozzi L, Staveland B, Holt-Gosselin B et al., 2020.The Human Connectome Project for Disordered Emotional States: Protocol and Rationale for a Research Domain Criteria Study of Brain Connectivity in Young Adult Anxiety and Depression.Neuroimage 214:116715. doi: 10.1016/j.neuroimage.2020.116715.

165. Van den Berg NS, Huitema RB, Spikman JM et al., Impairments in Emotion Recognition and Risk-Taking Behavior After Isolated, Cerebellar Stroke**.**Cerebellum 19(3):419-425 doi: 10.1007/s12311-020-01121-x.

166. O'Donoghue J.L., Watson, G.E., Brewer, R., et al., 2020. Neuropathology associated with exposure to different concentrations and species of mercury: A review of autopsy cases and the literature. Neurotoxicology. 78, 88-98. https://doi.org/10.1016/j.neuro.2020.02.011

167. Karanth, S., Nelson, P.T., Katsumata, Y., et al., 2020. Prevalence and clinical phenotype of quadruple misfolded proteins in older adults. *JAMA Neurol*. 2020, e201741. https://doi.org/10.1001/jamaneurol.2020.1741.

168. Geser, F., Fellner, L., Haybaeck, J., Wenning, G.K., 2020. Development of neurodegeneration in amyotrophic lateral sclerosis: From Up or Down? J. Neural Transm (Vienna). https://doi.org/10.1007/s00702-020-02213-y.

169. Tomé, S.O., Vandenberghe, R., Ospitalieri, S., et al., 2020. Distinct molecular patterns of TDP-43 pathology in Alzheimer's disease: relationship with clinical phenotypes. Acta Neuropathol Commun. 8,61. https://doi.org/10.1186/s40478-020-00934-5.

170. Bove, C., Travagli, R.A., 2019. Neurophysiology of the brain stem in Parkinson's disease. J. Neurophysiol. 121, 1856-1864. https://doi.org/10.1152/jn.00056.2019.

171. Váradi, C., 2020. Clinical features of Parkinson's disease: The Evolution of Critical Symptoms. Biology (Basel). 9, E103. https://doi.org/10.3390/biology9050103.

172. Custodio, N., Wheelock, A., Thumala, D., Slachevsky, A., 2017. Dementia in Latin America: Epidemiological Evidence and Implications for Public Policy. Front. Aging. Neurosci. 9, 221. https://doi.org/10.3389/fnagi.2017.00221.

173. Casterton, R.L., Hunt, R.J., Fanto, M., 2020. Pathomechanism heterogeneity in the amyotrophic lateral sclerosis and frontotemporal dementia disease spectrum: Providing

Focus Through the Lens of Autophagy. J. Mol. Biol. 432, 2692-2713. https://doi.org/10.1016/j.jmb.2020.02.018.

Figure description

Figure 1

Trend of maxima $PM_{2.5}$ 24-hour average concentrations registered in all monitoring stations of the MMC from 2004 to April 2020 and their comparison against the WHO daily mean average (blue solid line) and the US AQI. Data correspond to measurements from the manual PM network of the SEDEMA under a 6-day sampling schedule. Source: http://www.aire.cdmx.gob.mx/default.php#

Figure 2

Immunohistochemistry representative substantia nigrae pars compacta (SNpc) and brainstem sections from subjects in 1st through 6th decades of life. A. SNpc neuron with positive pτ nuclei and a few granular deposits of pτ in perinuclear location in the neuron in Insert. Immunohistochemistry/IHC xAT8, 3,3'-diaminobenzidine DAB/IHC, brown product. Scale bar 10um and 50 μm in the insert. B and C correspond to SNpc neurons in an 11month old baby stained with TDP-43.In B the neurons marked by arrows show strong nuclear staining (Scale bar 50 μm), while in C we have a neuron with strong nuclear DTP immunoreactivity (short arrow) contrasting with one with loss of nuclear TDP expression (arrow head)Scale bar 10 μm. IHC TDP-43, DAB, brown product. D. Same 11m old baby with a diffuse amyloid plaque in frontal cortex. IHC Aβ, red product. E and F IHC pτ and DAB.E. 17y old male SNpc pτ +neurites marked by arrows while a neuron is marked by *.F corresponds to SNpc in a 11y old female, a long pτ + neurite is marked by short arrows and adjacent neurons are identified by arrow heads. G. 17y old male, same as in E showing

two III motor cranial neurons, the one on the upper left one shows a pτ + nucleus (arrowhead), while the right one (short arrow), is negative. IHC pτ and DAB (Scale bar 10 um).H same as F,11y old female frontal cortex with a blood vessel(bv) with extensive wall amyloid extending into the adjacent neuropil(arrows). Frontal neurons with intracytoplasmic Aβ are marked with arrow heads. IHC Aβ and red product (Scale bar 50 μm).I.17y old frontal cortex with a diffuse Aβ plaque IHCAβ and red product (Scale bar 50 μm).J.13y old female SNpc positive neurons to αSyn, the short arrows point to the + αS granules, the arrow head to the neuromelanin. Insert shows one strongly + αSyn lower brainstem pigmented neuron in the same child. The arrow head point to the neuromelanin and the short arrows to the + αSyn. IHC x αS and red product (Scale bar 10 um).K.14y old male with a +TDP-43 neuron in pontine reticular formation,the immunoreactive + particles are mostly in the vicinity of the nucleus (arrow heads), there is nuclear clearing (long arrow). The insert shows the presence of glial cytoplasmic + inclusions with coiled body-like morphology (arrows). IHC TDP-43 DAB (Scale bar 50um). L.36y old frontal cortex with both diffuse (long arrow) and mature (short arrow) Aβ plaques and GFAP reactive astrocytes close-by. IHC Aβ and GFAP Red product/DAB for GFAP (Scale bar 10 μm).M 40 y old male with SNpc with numerous neurons with neurofibrillary tangles (arrow heads), long + neurites(short arrows) and free tangle neurons(long arrows). IHC pτ and DAB (Scale bar 50 μm).N 32y old female SNpc with + granular cytoplasmic αSyn IHC αSyn and red product (Scale bar 10 μm).O. 50y male SNpc with a Lewy-body like structure in a heavily degranulated neuron(arrow), an adjacent neuron (arrow head) shows unremarkable neuromelanin. ICH x αS and red product (Scale bar 10 um). P. 27y old male SNpc shows a heavily degranulated neuron (arrow heads) with a TDP-43 nuclear clearing (arrow). IHC TDP-43 red product (Scale bar 10μm). Q and R show 2 SNpc neurons in an

11y boy with significant cell damage and macrophages ingesting neuromelanin(Q).S, T and U are SNpc neurons from a 14y old boy with a small number of neuromelanin granules in the midst of a disintegrating cytoplasm and in proximity with macrophages and capillaries. In T the neuron show a typical hyaline cytoplasmic inclusion and in the upper right quadrant a macrophage nuclei show clumping of the chromatin (arrowhead) V. 14y old female with a pigmented locus coeruleus neuron showing cytoplasm disintegration and an attached macrophage(arrowhead).W. 15y old male with SNpc neurons with abundant NM and an attached macrophage ingesting NM(arrowhead).X. 22y old female, 2 SNpc neurons, the one on the lower quadrant shows an ill-defined cytoplasm and two nuclei likely from microglial cells, while the upper shows a ghost neuron with a fibrillary ill defined structure and a few NM granules. Y. 36y old male with a low power view of the SNpc to look at the numerous neurons with no NM (long arrows) at all contrasting with some with NM granules(short arrows).Macrophages among the degranulated neurons are marked with arrowheads. Z Same 36y male with close-up of the area with macrophages (arrowheads) and the severely damaged neurons (long arrows).

Figure 3

Neurovascular Unit (NVU) in the substantia nigrae. Small blood vessels, including capillaries and small arterioles exhibited abnormal walls with activated endothelial cells (ECs) and leaking walls. A. Three small blood vessels are seen with leaking walls with clusters of lipids in the neuropil. The neuropil is vacuolated and fragments of cells are seen around blood vessels. Lipofuscin is seen in smooth muscle cells and pericytes. B. Three y old male SNpc capillary surrounded by a fragmented neuropil (*). Perivascular astrocyte end-feet appear dissociated from the capillary wall. An intact RBC is in the lumen.

Extensive areas of vacuolated neuropil with few axons remain.C. SNcp neuropil in a 12y male, note the patchy vacuolated and fragmented neuropil (*).Axons of different sizes and thickness of myelin show focal fragmentation. D. A close-up of a blood vessel in an area close to the one shown in C. Note the close contact between the RBC and the endothelial surface. The arrow heads show the contact area and the presence of nanoparticles (NPs). NPs are also seen in the endothelial cell nucleus (arrows)in close contact with the heterochromatin.

Figure 4

Substantia nigrae representative electron micrographs from 1st through 3rd decades of life.

A. Eleven m old with a SNpc neuron with very few neuromelanin (NM) structures but already significant damage to the neuropil i.e., large vacuolated spaces with debri, fragments of macrophage-like cells (MΘ) and few axons.

B. Same neuron as in A to show the few NM (arrows) and an abundant endoplasmic reticulum (ER).

C.Twelve y old SNpc neuron with a cluster of NM in a paranuclear location. Note the close contact of axons around this neuron with only a few, small areas of loosening neuropil(*).

D.A close-up of the NM cluster to show the uniform size between rough endoplasmic reticulum RER.

E. In the same neuron, a close-up of the nucleus and nucleolus and the loosing of the neuropil adjacent to the neuron cell membrane (*).

F. It is clear the presence of NPs in close contact with heterochromatin (arrows) and the double nuclear membrane with NPs at the intersection (arrowhead). Numerous small mitochondria (M) have fragmented cristae.

G. Fifteen y old NM close-up adjacent to dilated ER and abnormal mitochondria (M). Inside the NM we observe NPs (arrows) and lipid structures (lf).

H.Same as G to show another NM with NPs (white arrows) and mitochondria with NPs inside (black arrow) and dilated ER.In the Insert a close contact between the NM and a mitochondria, a relationship expected between a mitochondria and ER, not a NM.

I.Abundant and dilated RER with NPs inside (arrow).

J. Oligodendroglia are exhibiting fragmentation (*) and its surrounding axons vary in size and thickness of the myelin.

K. Twenty-six y old SNpc to show a distinct fibrillary structure with NPs (arrows) in the midst and closely attached to a lipid lipofuscin like structure.

L.An area with dilated ER and abnormal mitochondria. In the close contact between the dilated ER and the small mitochondria (arrowhead) the resultant MERC is abnormal.

Figure 5

Substantia nigrae representative electron micrographs from beyond 5^{th} decade of life.

A. Seventy-one y old MMC resident substantia nigrae, 1μm toluidine blue section showing substantia nigrae pars compacta neurons with abundant cytoplasmic neuromelanin (NM) (long arrows) in sharp contrast with neurons with scanty cytoplasm, few NM and small nuclear fragments (arrowheads). Blood vessels are marked with an L in their lumen and some small vessels have a vacuolated perivascular neuropil (*).

B. Same subject as A, this neuron shows abundant NM and several macrophage-like cells around. The lower macrophage nucleus (arrowhead) shows a pyknotic nucleus, while the upper two (long arrows) exhibit an intact nuclear membrane but their cytoplasm is fragmented.

C.At greater magnification, is clear the neuronal cytoplasm is vacuolated and there are clearing of the cytoplasm around a disrupted nucleus. The neuronal inclusion with dysmorphic organelles is adjacent to the empty space (*).

D.The intracytoplasmic inclusion characterized by filaments, membrane fragments, dysmorphic organelles and lipids (Shahmoradian et al., 2019) is marked by several arrows.

E.A small blood vessel in the vicinity of the neuron in B-D, with a RBC in the lumen and a tight junction (Tj) (arrow) in the endothelial cell.

F. The Tj at higher power shows a common finding in substantia nigrae endothelial cells: the abundant nanoparticles decorating the structure (arrow).

G. Cell nuclei with numerous NPs both in the heterochromatin (arrows) and in the nuclear matrix(arrowheads).

H. Small blood vessel with a lumen (L) and abundant lipofuscin in close contact with beta β-pleated sheet twisted tubules (arrows). A cluster of cross section sheet in close contact with a lipid portion of lipofuscin (arrowheads).

I.Perineuronal macrophages are very common in older subjects and contain numerous lysosomes and rare structures with a lattice image(arrow).

J. At higher magnification, the lattice image has 10 layers of well ordered fringes with a perpendicular alignment(arrows).

Figure 6

SNpc electron micrographs of a 32y old male corresponding to Figures 7 and 8.

A. The neurovascular unit in this individual is abnormal, with neuropil breakdown (*) and the perivascular astrocyte end-feet dissociating from the capillary wall. In close contact with the blood vessel (arrowhead) an elongated fragment of a macrophage-like cell(M) is remarkable. Its cytoplasm is dark and shows numerous vacuoles (v). Nanoparticles are seen

in various locations, within the wall of the capillary (black arrow) and in empty neuropil (double arrow).

B.SNpc neuron with NM granules and RER.Note the numerous NPs in different organelles within the cell (short arrows), including within the NM.The mitochondria show abnormal cristae and the spaces between the ER and other organelles exhibits vaculated, empty areas (*).

C.The abnormal mitochondria show numerous NPs, of different sizes within the cristae, matrix and double membrane. ER structures are dilated and short.

Figure 7 A, B. High magnification high-angle annular dark field-scanning/transmission electron microscopy (HAADF-STEM) of SN tissue, 32 y old subject (also please see Figure 8); B: a higher magnification image of the bright, electrodense NPs (marked as 1, 2 and 3) shown in the area in the white box in A. C. EDXA spectrum for the area shown in B. D – F. elemental maps for the area shown in B.

Figure 8. A and F: HAADF-STEM of NPs around a mitochondrion in SN tissue, 32 y old subject (B and G higher magnification images of the bright, electrodense NPs shown in the white box in A and F, respectively); C – E: elemental maps for the particles in the white box shown in A; H – J: elemental maps for the area shown in F.

Figure 9A and B:HAADF-STEM of Ti-bearing elongated laths, in neuroenteric tissue sample from a 39y old male with both AD and PD hallmarks; C EDX spectrum for the area imaged in A and B (NB Cu peaks reflect the use of a copper TEM support grid).

Figure 10. Room-temperature SIRM values versus age for A. SN samples, B. ectum/tegmentum/PAG, C. cerebellum, and D. box plots, showing significant differences between the magnetic content of the 3 regions (Kruska-Wallis test, p-value = 0.0116).

Table 1

Table 1. Room temperature SIRM values for a representative sub-cohort of the MMC subjects, and calculated concentrations and number concentrations of magnetite NPs: SN = substantia nigra; TTP = tectum/tegmentum/PAG; CB = cerebellum.

ID#	Age	SIRM (10^{-6} Am^2 Kg^{-1})			Magnetite concentration µg/g			No. magnetite particles 10^9/g		
		SN	*TTP*	*CB*	*SN*	*TTP*	*CB*	*SN*	*TTP*	*CB*
1	12	1.8	3.92	3.31	0.13	0.28	0.24	1.61	3.52	2.97
2	15	1.36	13.7	6.05	0.10	0.99	0.44	1.22	12.30	5.43
3	15	9.37		0.3	0.68		0.02	8.41		0.27
4	17	1.52	0.5		0.11	0.04		1.36	0.45	
5	17	0.53	4.57		0.04	0.33		0.48	4.11	
6	20	36.23	15.32	10.16	2.63	1.11	0.74	32.52	13.75	9.12
7	20	1.02	0.63	2.11	0.07	0.05	0.15	0.91	0.57	1.89
8	20			0.5			0.04			0.45
9	20			3.37			0.24			3.02
10	22	0.52	0.87	30.2	0.04	0.06	2.19	0.47	0.78	27.11
11	23	1.37		6.07	0.10		0.44	1.23		5.45
12	24	1.02	5.55	1.03	0.07	0.40	0.08	0.92	4.99	0.93
13	24	0.89	0.95	4.49	0.07	0.07	0.33	0.80	0.85	4.03
14	26	0.6	3.37	0.69	0.04	0.24	0.05	0.54	3.02	0.62
15	26	4.08	0.49	11.72	0.30	0.04	0.85	3.67	0.44	10.52
16	27	0.53	1.02		0.04	0.07		0.47	0.92	
17	29	1.9	24.73		0.14	1.79		1.70	22.20	
18	31		3.97	4.08		0.29	0.30		3.56	3.66
19	31	1.54	5.72	15.93	0.11	0.41	1.15	1.38	5.13	14.30
20	32	2.95	2.97	5.01	0.21	0.22	0.36	2.65	2.67	4.50
21	34			2.84			0.21			2.55
22	35			14.25			1.03			12.79
23	36	2.35	1.39		0.17	0.10		2.11	1.25	
24	39	0.9	8.78	6.51	0.07	0.64	0.47	0.81	7.88	5.85
25	45	1.1	1.99	1.32	0.08	0.14	0.10	0.99	1.79	1.19
26	50	2.07	3.91	6.47	0.15	0.28	0.47	1.86	3.51	5.81
27	61	0.2	1.86		0.02	0.14		0.18	1.67	
28	71	3.62	4.92	18.46	0.26	0.36	1.34	3.25	4.42	16.57
29	75	0.29	1.96		0.02	0.14		0.26	1.76	
30	75	2.64	1.22		0.19	0.09		2.37	1.09	
31	85	5.23	0.34		0.38	0.03		4.69	0.31	

Figure 1

Click here to access/download;Figure;Figure1.TIF

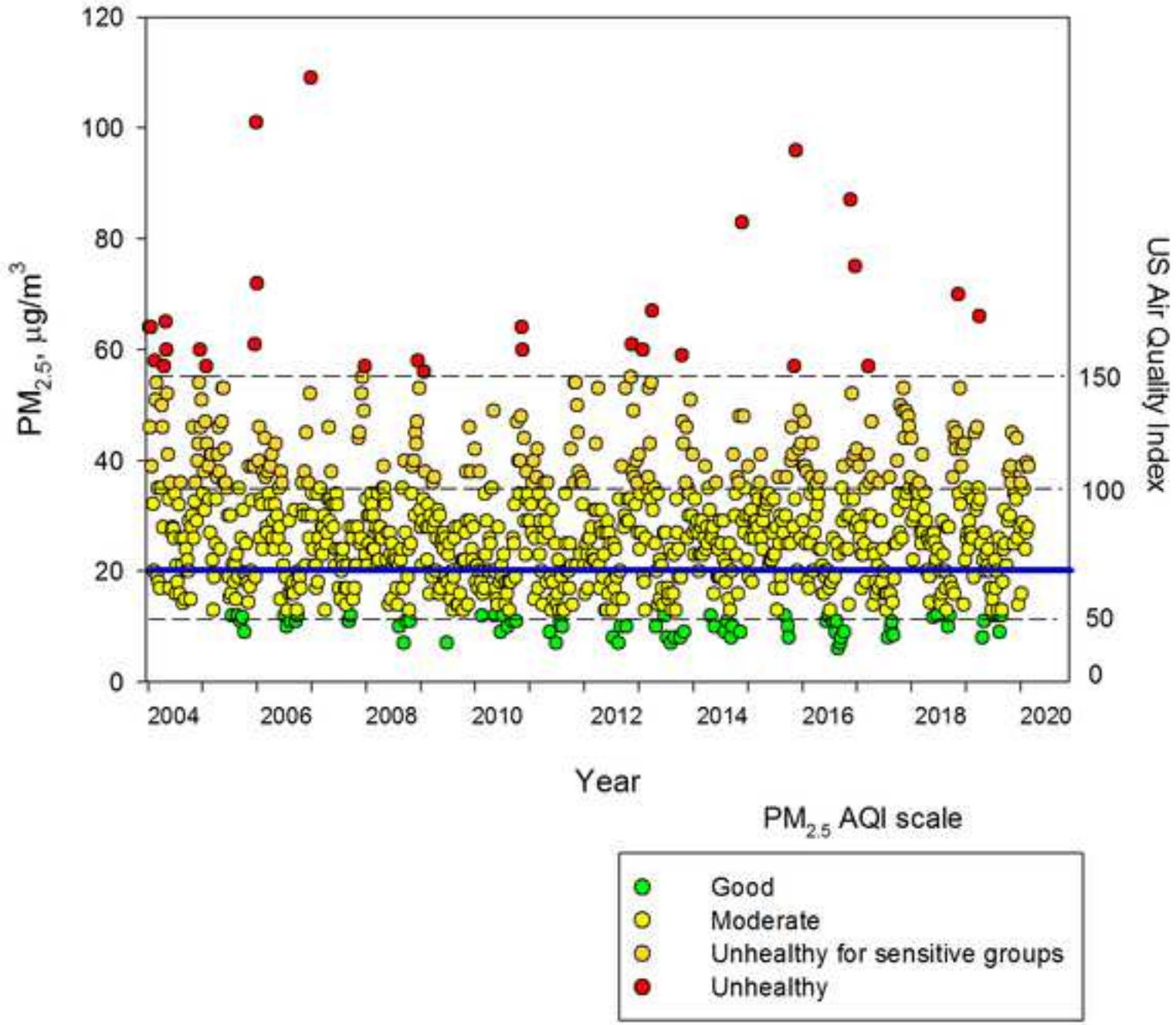

Figure 2

Click here to access/download;Figure;FIGURE2.tif

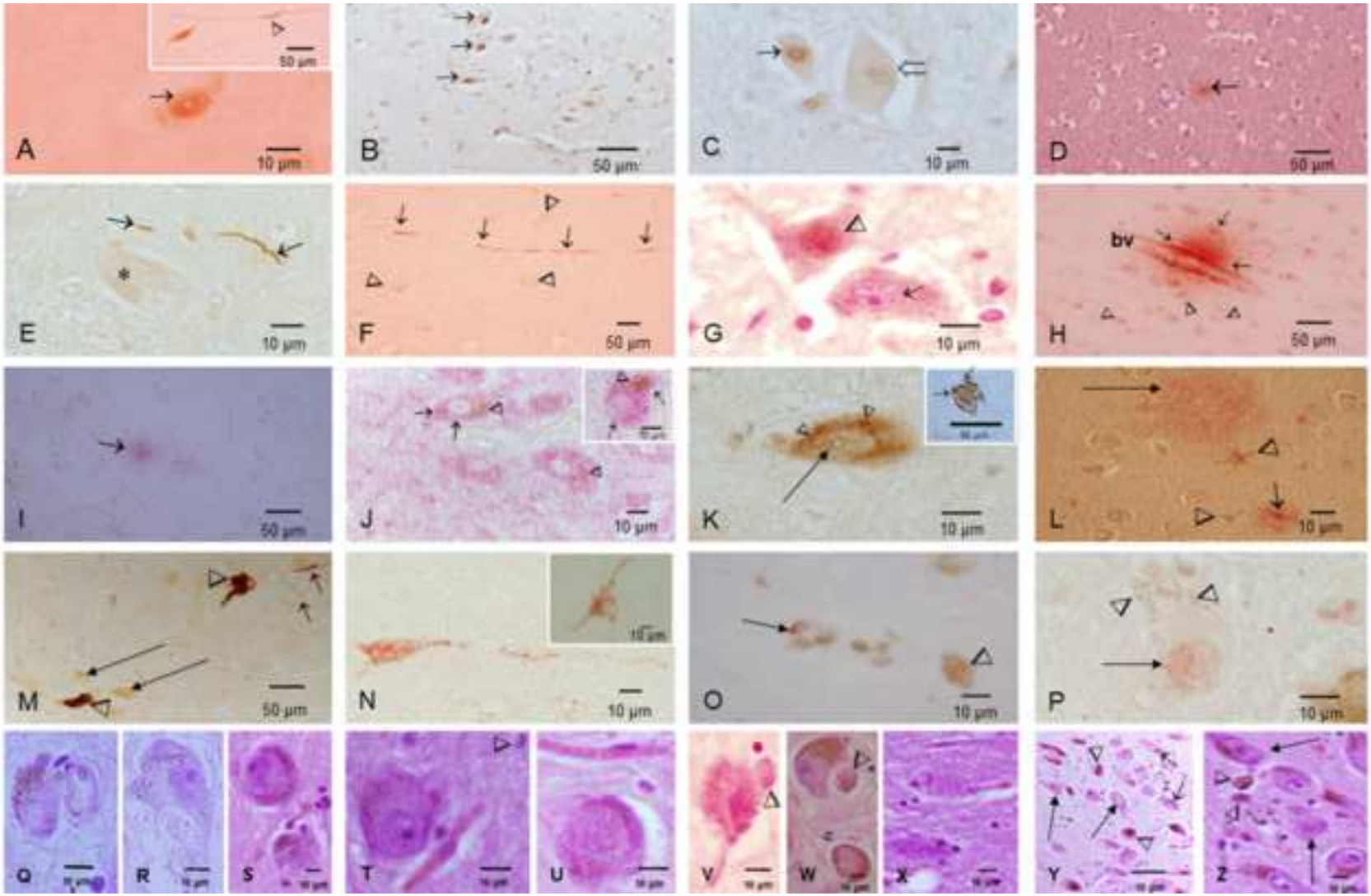

Figure 3

Click here to access/download;Figure;FIGURE3.tif

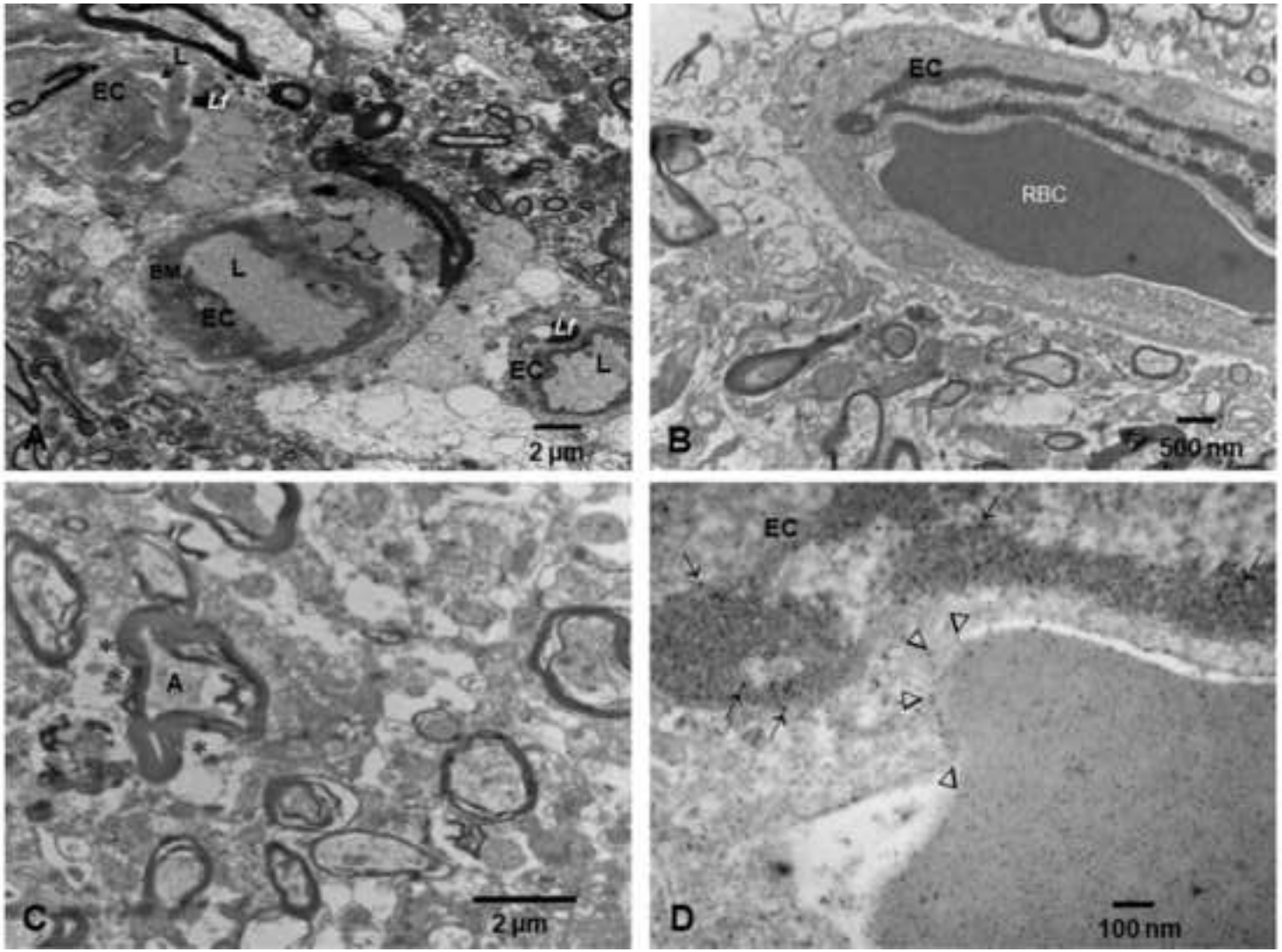

Figure 4

Click here to access/download;Figure;FIGURE4.tif

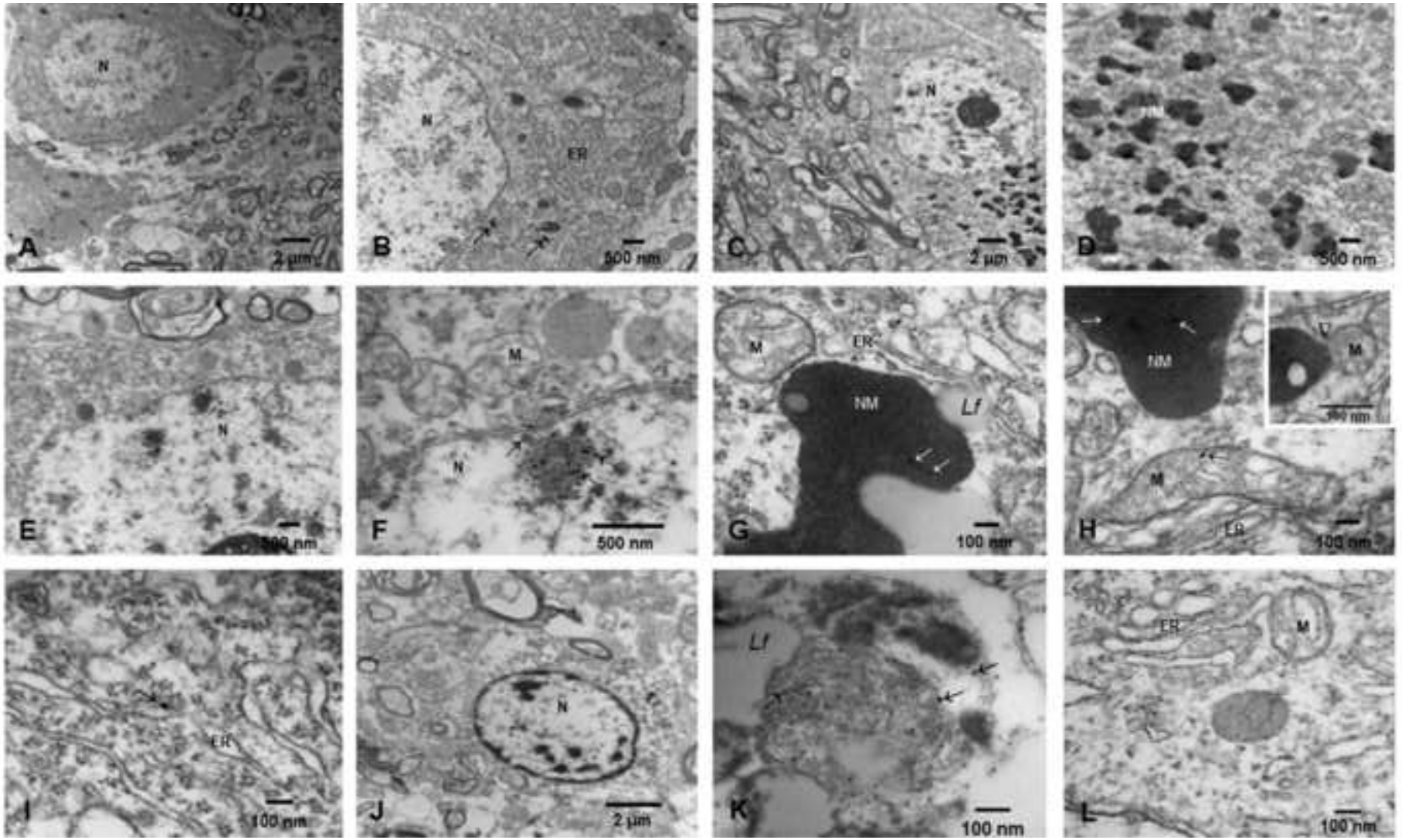

Figure 5

Click here to access/download;Figure;FIGURE5.tif

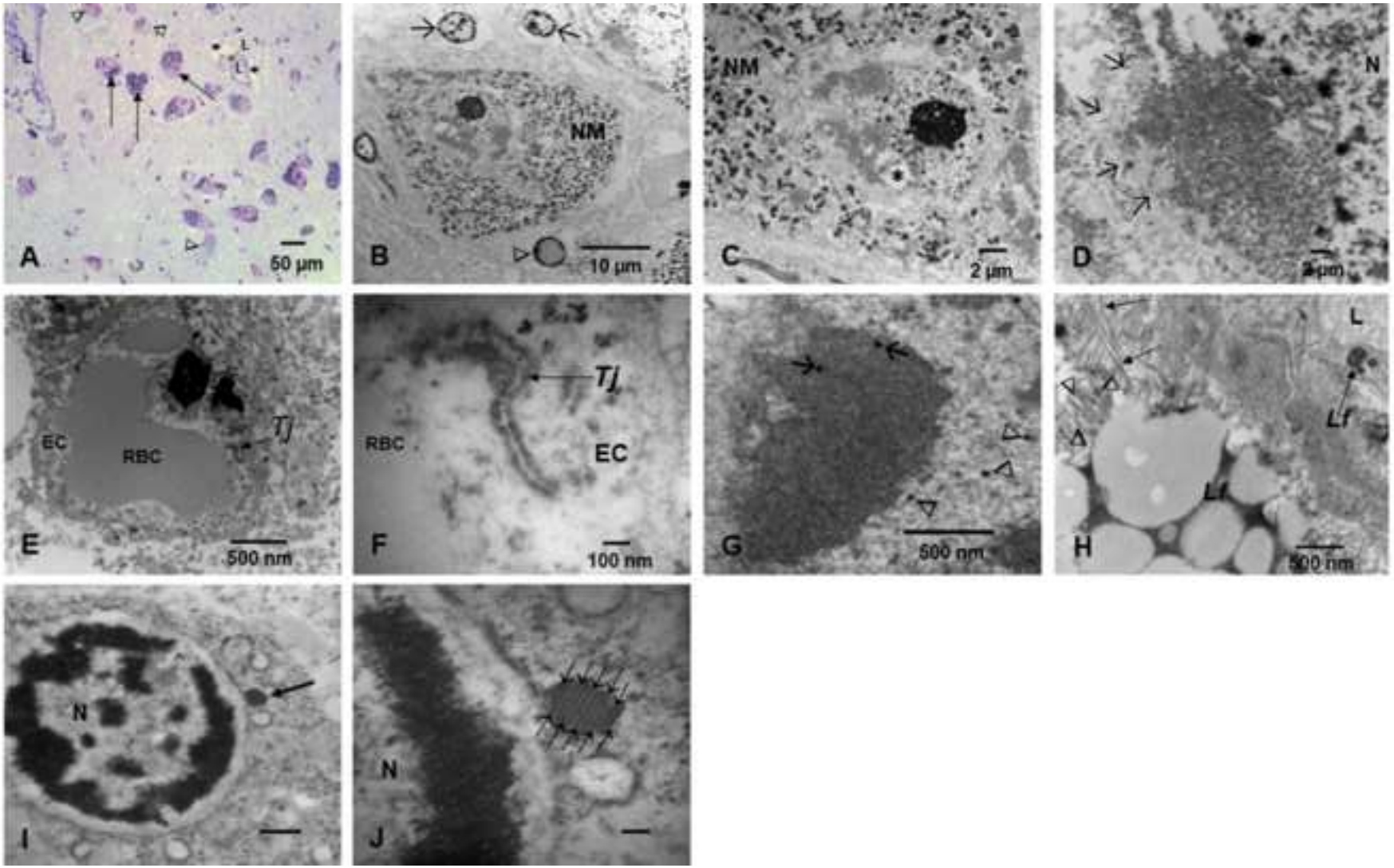

Figure 6

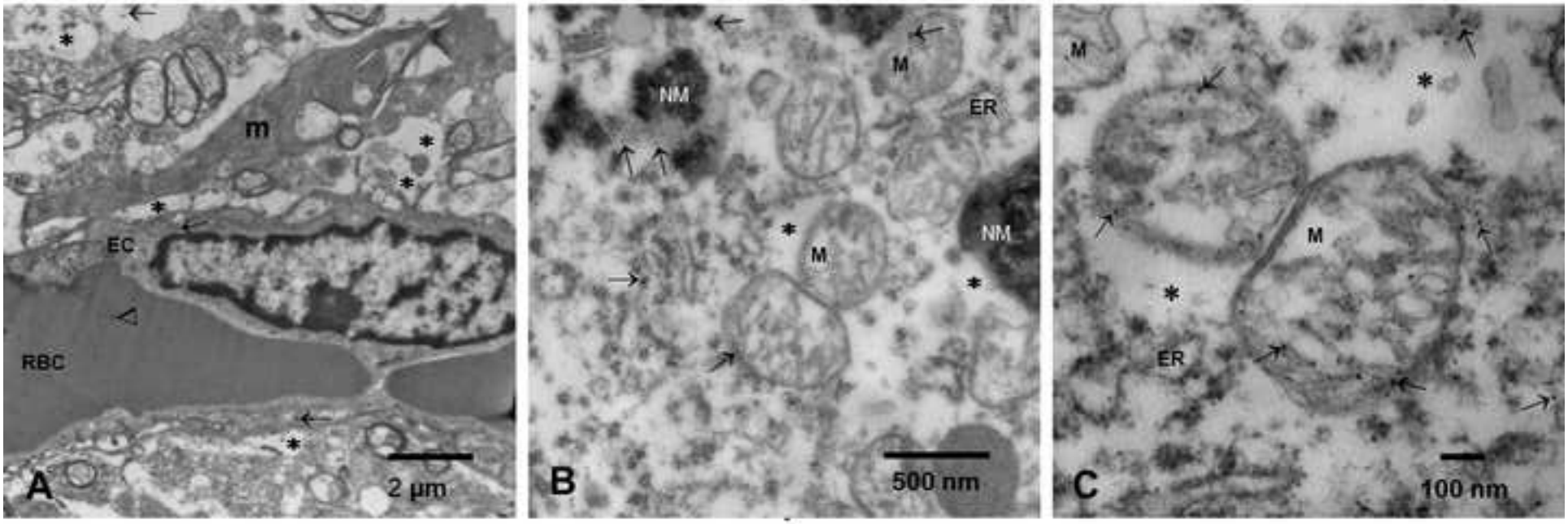

Figure 7

Click here to access/download;Figure;FIGURE7.jpg

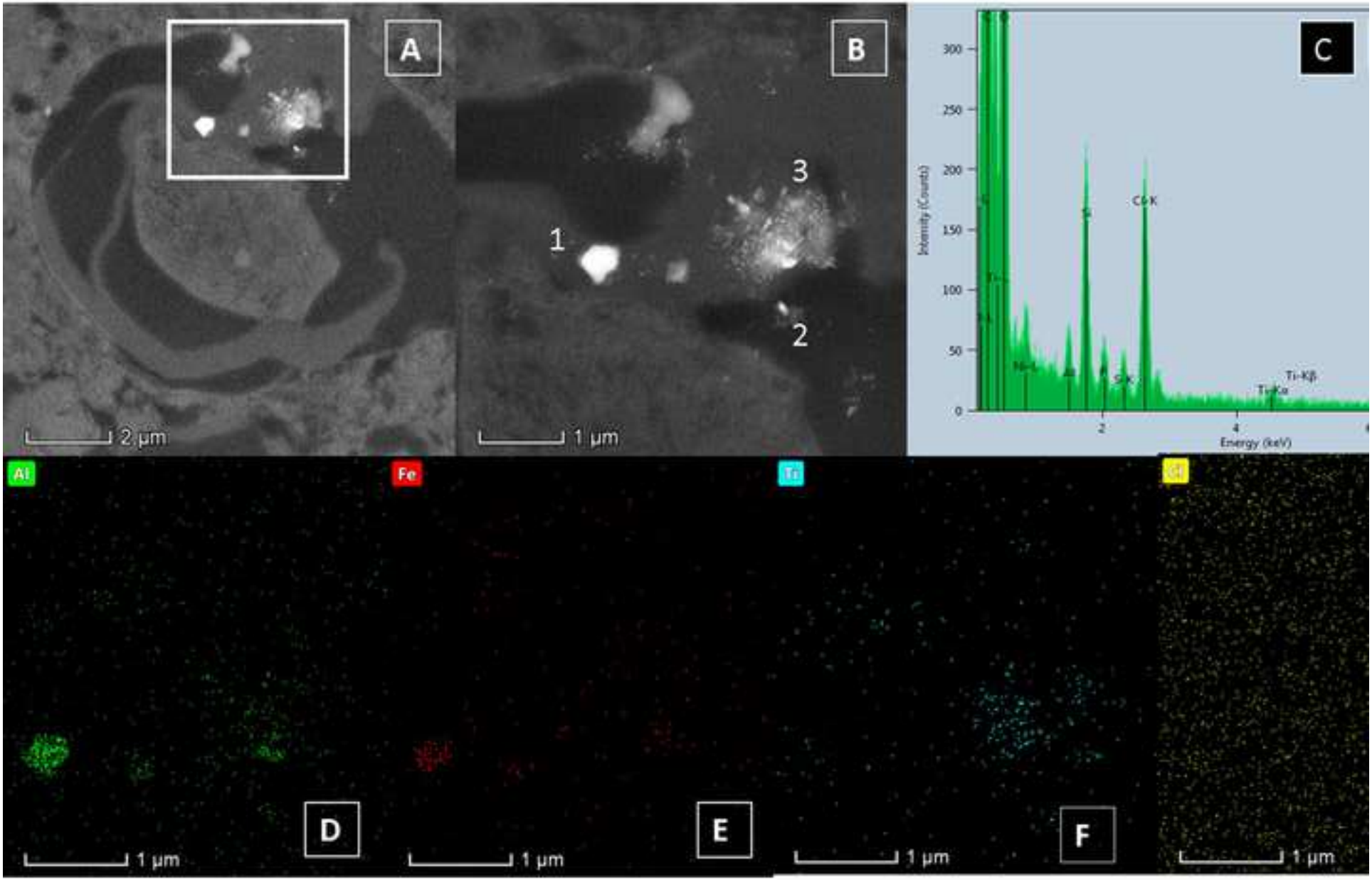

Figure 8

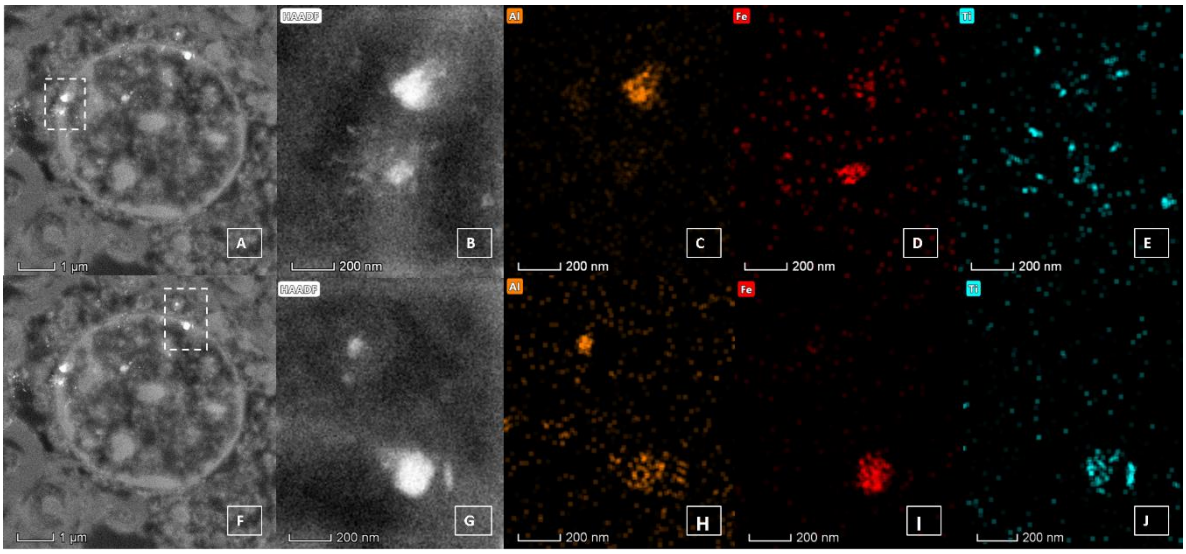

Figure 8. A and F: HAADF-STEM of NPs around a mitochondrion in SN tissue, 32 y old subject (B and G higher magnification images of the bright, electrodense NPs shown in the white box in A and F, respectively); C – E: elemental maps for the particles in the white box shown in A; H – J: elemental maps for the area shown in F.

Figure 9

Click here to access/download;Figure;FIGURE9.jpg

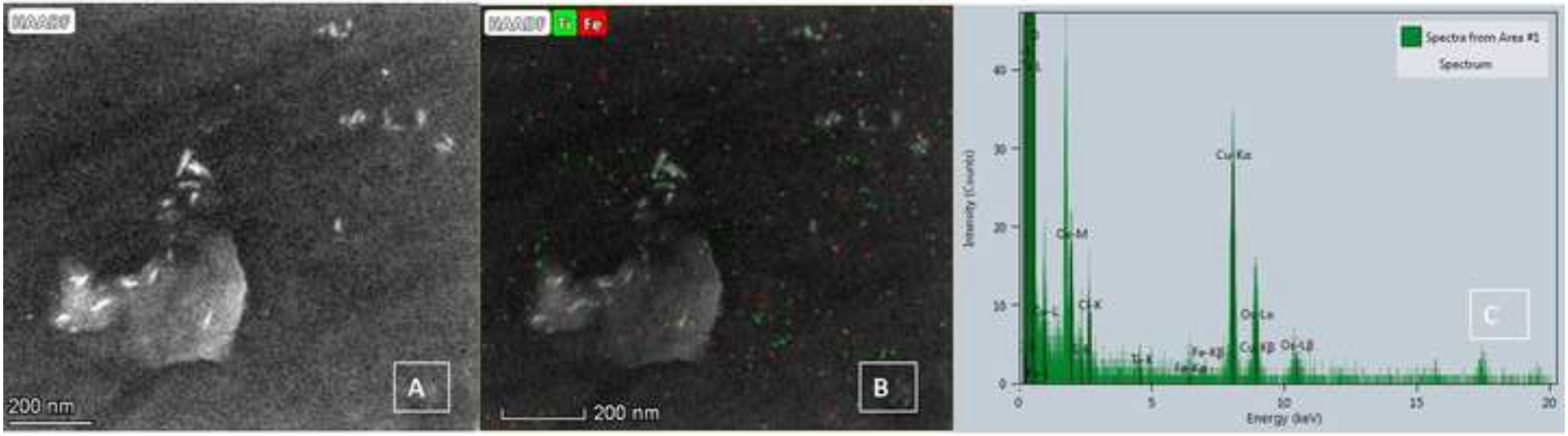

Figure 10

Click here to access/download;Figure;FIGURE10.jpg

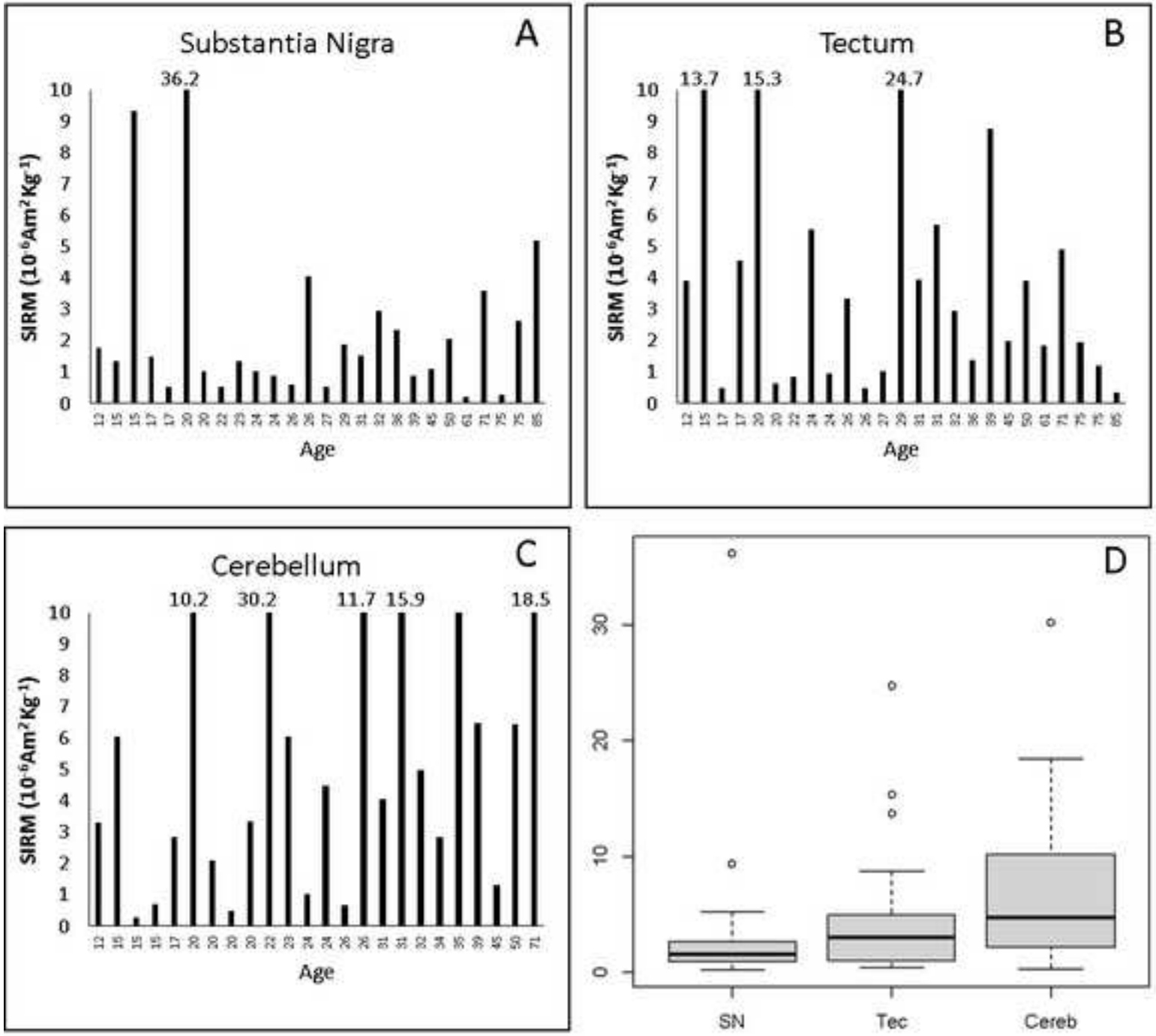

CRediT author statement

Calderón-Garcidueñas Lilian: Conceptualization, data curation, formal analysis, Methodology, Investigation, Original draft preparation, Writing- Reviewing and Editing, Visualization, Supervision, Project administration. **Angélica González-Maciel, Rafael Reynoso-Robles, Randy Kulesza, Ingolf Lachmann, Ricardo Torres-Jardón, Partha S. Mukherjee:** Formal analysis, Visualization, Investigation, Supervision, Validation, Writing- Reviewing and Editing **Barbara Maher**: Data curation, formal analysis, writing- reviewing and editing, visualization. SIRM, HRSTEM and EDX. HAADF-STEM images. **J. Hammond:** formal analysis, visualisation, investigation and validation.

Conflict of Interest Statement

None of the authors have any conflict of interest